Quantification of regional terrestrial biosphere CO_2 flux errors in v10 OCO-2 MIP ~~models~~ensemble using airborne measurements

Jeongmin Yun[1*], Junjie Liu[1*], Brendan Byrne[1], Brad Weir[2], Lesley E. Ott[2], Kathryn McKain[3], Bianca Baier[3], Luciana V. Gatti[4], Sebastien C. Biraud[5]

[1]Jet Propulsion Laboratory, California institute of Technology, Pasadena, CA 91109, USA
[2]NASA Goddard Space Flight Center, Greenbelt, MD 20771, USA
[3]NOAA Global Monitoring Laboratory, Boulder, Colorado, USA
[4]General Coordination of Earth Science (CGCT), National Institute for Space Research (INPE), São José dos Campos, Brazil
[5]Lawrence Berkeley National Laboratory, Berkeley, California, USA

Correspondence to: Jeongmin Yun (jeongmin.yun@jpl.nasa.gov) and Junjie Liu (junjie.liu@jpl.nasa.gov)

Abstract. Multi-inverse modeling inter-comparison projects (MIPs) provide a chance to assess the uncertainties in inversion estimates arising from various sources such as atmospheric CO_2 observations, transport models, and prior fluxes. However, accurately quantifying ensemble CO_2 flux errors remains challenging, often relying on the ensemble spread as a surrogate. This study proposes a method to quantify the errors of regional terrestrial biosphere CO_2 flux estimates from 10 inverse models within the Orbiting Carbon Observatory-2 (OCO-2) MIP by using independent airborne CO_2 measurements for the period 2015–2017. We first calculate the root-mean-square error (RMSE) between the ensemble mean of posterior CO_2 concentration estimates and airborne observations and then isolate the CO_2 concentration error caused solely by the ensemble mean of posterior terrestrial biosphere CO_2 flux estimates by subtracting the errors of observation and transport in seven regions. Our analysis reveals significant regional variations in the average monthly RMSE over three years, ranging from 0.~~90~~88 to ~~2.04~~1.91 ppm. The ensemble flux error projected into CO_2 space is a major component that accounts for ~~58-84~~55-85% of the mean RMSE. We further show that in five regions, the observation-based error estimates exceed the ~~atmospheric CO_2 errors computed from the~~ ensemble spread of posterior CO_2 ~~flux estimates~~ errors by 1.~~37~~33-1.~~89~~93 times, implying an underestimation of the actual ensemble flux ~~error~~errors, while their magnitudes are comparable in two regions. By identifying the most sensitive areas to airborne measurements through adjoint sensitivity analysis, we find that the underestimation of biosphere flux errors is prominent in eastern parts of Australia and East Asia, western parts of Europe and Southeast Asia, and midlatitude North America~~, suggesting~~ where the ~~presence~~magnitudes of ~~systematic biases related to anthropogenic CO_2~~annual fossil fuel emissions ~~in inversion estimates.~~exceed those of annual biosphere fluxes by 3-31 times over the three years. The regions with no underestimation ~~were~~are southeastern Alaska and northeastern South America where fossil fuel emissions are comparable to or less than biosphere fluxes. Our study emphasizes the value of independent airborne measurements not only for the overall evaluation of inversion performance but also for quantifying regional errors in ensemble terrestrial biosphere flux estimates.

1 Introduction

Understanding the sources and sinks of atmospheric CO_2 is essential for developing efficient strategies for climate change mitigation and accurate climate predictions. Terrestrial ecosystems have acted as major carbon sinks by absorbing around 30% of anthropogenic fossil and land-use CO_2 emissions over the past few decades (Friedlingstein et al., 2023). However, ~~the absorbed amount~~this uptake is highly variable both spatially and temporally as carbon exchange processes are sensitive to environment and climate change (Liu et al., 2017; Bastos et al., 2019; Piao et al., 2020). ~~To track changes in the terrestrial carbon sinks,~~ Accurate estimates of ~~the~~ regional terrestrial biosphere carbon fluxes and their uncertainties are, therefore, crucial for monitoring changes in terrestrial carbon sinks.

Atmospheric CO_2 inverse modeling is ~~one of the~~a widely employed approaches to estimate terrestrial and air-sea CO_2 fluxes ~~from~~by assimilating observed atmospheric CO_2 concentrations ~~by using a transport model and data assimilation techniques.~~. Most inverse modeling approaches are based on the Bayesian theory, wherein posterior flux ~~estimates are~~is estimated from prior knowledge and atmospheric CO_2 observations weighted by their uncertainties. This approach estimates a posterior probability distribution that can be represented as a maximum a posterori solution (referred to as $\hat{x}$~~),~~) and an error covariance matrix, following the notation of Rodgers (2000). Theoretically, since atmospheric CO_2 observations generally have lower uncertainty than prior terrestrial flux estimates, ~~greater observation data leads~~more observations lead to posterior fluxes approaching true values (Liu et al., 2014).

However, concerns have been raised that the inverse modeling results are sensitive to ~~systematic errors in~~the selection of transport models, prior flux datasets, and ~~inversion setups~~data assimilation techniques that are not accounted for in the Bayesian framework (Basu et al., 2018; Philip et al., 2019; Schuh et al., 2019). In order to obtain more robust terrestrial flux estimates and assess their uncertainties resulting from various sources (e.g., atmospheric transport and assimilation techniques), inverse modeling intercomparison projects (MIPs) have been conducted. These projects include the TransCom project (Gurney et al., 2004; Houweling et al., 2015), which was first initiated in ~~1998~~1990s, as well as subsequent projects such as the Global Carbon Project (GCP; Friedlingstein et al., ~~2023), the REgional Carbon Cycle Assessment and Processes (RECCAP~~2023; Ciais et al., 2022~~),~~) and the Orbiting Carbon Observatory-2 (OCO-2) MIP (Crowell et al., 2019; Peiro et al., 2022; Byrne et al., 2023). These MIPs involve different inverse modeling groups using state-of-the-art transport modeling and assimilation techniques that assimilate in situ and satellite CO_2 data. Through these MIPs, researchers have analyzed differences in the maximum posteriori solution across models. The OCO-2 MIP has revealed a general agreement on global flux estimates among ensemble models, but significant discrepancies in regional fluxes, regardless of whether in-situ and/or satellite data are assimilated (Crowell et al., 2019; Peiro et al., 2022).

Realistic error quantification of posterior fluxes from atmospheric flux inversions is essential ~~to understand~~for understanding how well the regional fluxes are constrained by current CO_2 observing network and identify regions with high uncertainty, allowing us to prioritize efforts to mitigate the error. The Bayesian formulation provides a method for calculating uncertainties on posterior fluxes based on ~~prior uncertainties and~~ uncertainties in ~~the~~ prior fluxes and assimilated data. This can be calculated analytically or approximated using a Monte Carlo method for variational methods (Chevallier et al., 2007; Feng et al., 2009; Liu et al., 2014), however, this is often computationally prohibitive for many inversion systems. This Bayesian posterior uncertainty accounts for random errors in the prior fluxes and observations but does not explicitly incorporate systematic errors, thus providing a potential underestimate of the total posterior error.

Errors in ~~posterior~~the maximum a posteriori fluxes are also commonly characterized through comparisons between independent atmospheric CO_2 measurements and posterior atmospheric CO_2 (Houweling et al., 2015; Crowell et al., 2019; Byrne et al., 2023). This approach can provide insights into the biases of current inverse modeling at the global, latitudinal, or site-specific scales. However, as atmospheric CO_2 concentrations are influenced by both local and remote sources, it is difficult to identify regions where the observation-model comparison results are representative. Furthermore, these comparisons ~~do~~include not ~~indicate~~ only posterior flux errors, ~~as the differences between simulated and observed atmospheric CO_2 can arise from~~but also errors ~~of not only posterior fluxes, but also~~arising from transport, representation, and measurement. Because of these limitations, regional posterior flux errors of the ensemble mean have been generally defined as the ensemble spread among ensemble posterior fluxes, but this method ~~lacks~~does not have an observational and theoretical basis and may not reflect actual errors (Byrne et al., 2023).

~~Our~~This study aims to develop a framework to quantify the ~~error~~errors in regional terrestrial biosphere CO_2 fluxes ~~(from now on referred to as terrestrial CO_2 fluxes)~~ estimated from an ensemble of inverse models by using airborne CO_2 measurements, transport modeling, and adjoint sensitivity analysis. Our target ensemble results are derived from 10 ensemble members in the v10 OCO-2 MIP for the period 2015–2017, which provide both posterior CO_2 fluxes and posterior CO_2 concentrations sampled at observation sites and times. The ensemble assimilates OCO-2 column-averaged dry-air mole fraction (XCO_2) retrievals (ACOS v10; O'Dell et al., 2018) and in situ CO_2 measurements (Tohjima et al., 2005; Nara et al., 2017; Schuldt et al., ~~2022). We first analyze the spatiotemporal variations and relative magnitudes of various error components that necessitate consideration when comparing airborne CO_2 observations with the ensemble estimates of posterior atmospheric CO_2. Next, we calculate the CO_2 concentration errors caused only by posterior CO_2 fluxes by subtracting the errors of observations and transport from the observation-model differences with long-term observations in seven regions. Then, we identify the most sensitive areas represented by our evaluation results and quantify errors of the ensemble mean annual terrestrial CO_2 flux estimates in these areas.~~ 2021a; 2021b). This study uses more than 833,000 airborne CO_2 measurements collected at 1-5 km altitude above ground level (AGL) from 20 different measurement projects (e.g., Baier et al., 2021; Miller et al., 2021; NOAA Carbon Cycle Group ObsPack Team, 2018; Schuldt et al., 2021a; 2021b).

These data have broader spatial coverage and are less influenced by local sources compared to surface CO_2 data, thus capturing signals from regional surface CO_2 fluxes. We quantify the errors in ensemble mean estimates of posterior atmospheric CO_2 by comparing them with the airborne CO_2 data. We then estimate the contributions of various error components (e.g., representation, observation, transport, and flux errors) to the observation-model difference in atmospheric CO_2 and isolate the contribution of biosphere flux errors. Next, we identify the areas to which these airborne CO_2 are most sensitive to and quantify the annual biosphere flux errors in these areas.

2 Data and methodology

The aim of this study is to quantify the true errors of the ensemble terrestrial biosphere CO_2 fluxes generated by the v10 OCO-2 MIP ~~with~~using airborne observations. Here, "error" refers to the magnitude of the differences between the ~~observed~~true and estimated flux values, without considering the sign. To achieve this, we employ three steps of analysis as described in Figure 1. First, we define two quantities: 1) the root mean square errors (*RMSE*) between the ~~mean of~~ ensemble mean of posterior CO_2 concentrations and observed CO_2 ~~concentration~~concentrations, and 2) ~~an approximation of RMSE (~~ERR_{TOT}~~) defined as the sum of~~ (Section 2.3). $RMSE^2$ represents the true errors in OCO-2 MIP ensemble mean of CO_2 concentrations including representation errors (σ_r^2), observation errors ~~and errors in both~~ (σ_o^2), true flux ~~and~~ errors projected onto CO_2 concentration ($\sigma_{f_t}^2$), transport errors (σ_t^2), and error covariances between the preceding two terms ($cov(\sigma_{f_t}, \sigma_t)$). ERR_{TOT}^2 is the sum of the estimated error components, defined as the sum of ERR_{REP}^2, ERR_{OBS}^2 and ERR_{MIP}^2. ERR_{REP}^2 and ERR_{OBS}^2 indicate representation errors (σ_r^2) and observation errors (σ_o^2), respectively. ERR_{MIP}^2 is the sum of estimated flux errors projected onto CO_2 space (σ_{fe}^2) and transport errors (σ_t^2), and their error covariances ($cov(\sigma_{f_e}, \sigma_t)$), computed from an ensemble spread of posterior CO_2 concentrations ~~(Section 2.2).~~. Here we separate representation errors from transport errors for computational purpose. The ratio between ~~RMSE and~~ ERR_{TOT} and *RMSE* is then used to evaluate whether the estimated flux errors, computed from the ensemble spread of ~~ensemble~~ posterior fluxes ~~overestimates~~, overestimate or ~~underestimates~~underestimate the true errors in the ensemble mean fluxes. Next, we calculate ~~CO_2 uncertainties due to only the spread of OCO-2 MIP ensemble posterior fluxes (Section 2.3). With~~ the estimated flux ~~error~~errors projected onto atmospheric CO_2~~,~~ ($h(err_{f_e})$) through atmospheric transport simulations (Section 2.4). With $h(err_{f_e})$, ERR_{TOT}, and *RMSE*, we derive the true errors ~~of~~in ensemble mean of posterior fluxes ~~in~~projected onto CO_2 space ~~over seven regions.~~($h(err_{f_t})$). Then, we identify the areas ~~that~~where these airborne observations are most sensitive to using an adjoint sensitivity analysis and calculate the estimated posterior flux errors over ~~the area in flux space.~~these regions (err_{f_e}). Assuming a linear observation operator, the study finally computes the true errors of the ensemble mean posterior fluxes over the identified sensitive areas (err_{f_t}) by applying the ratio between ~~the true ensemble posterior errors~~$h(err_{f_t})$ and ~~the estimated ensemble posterior errors in CO_2 space~~$h(err_{f_e})$ to ~~the spread of ensemble posterior fluxes.~~err_{f_e}.

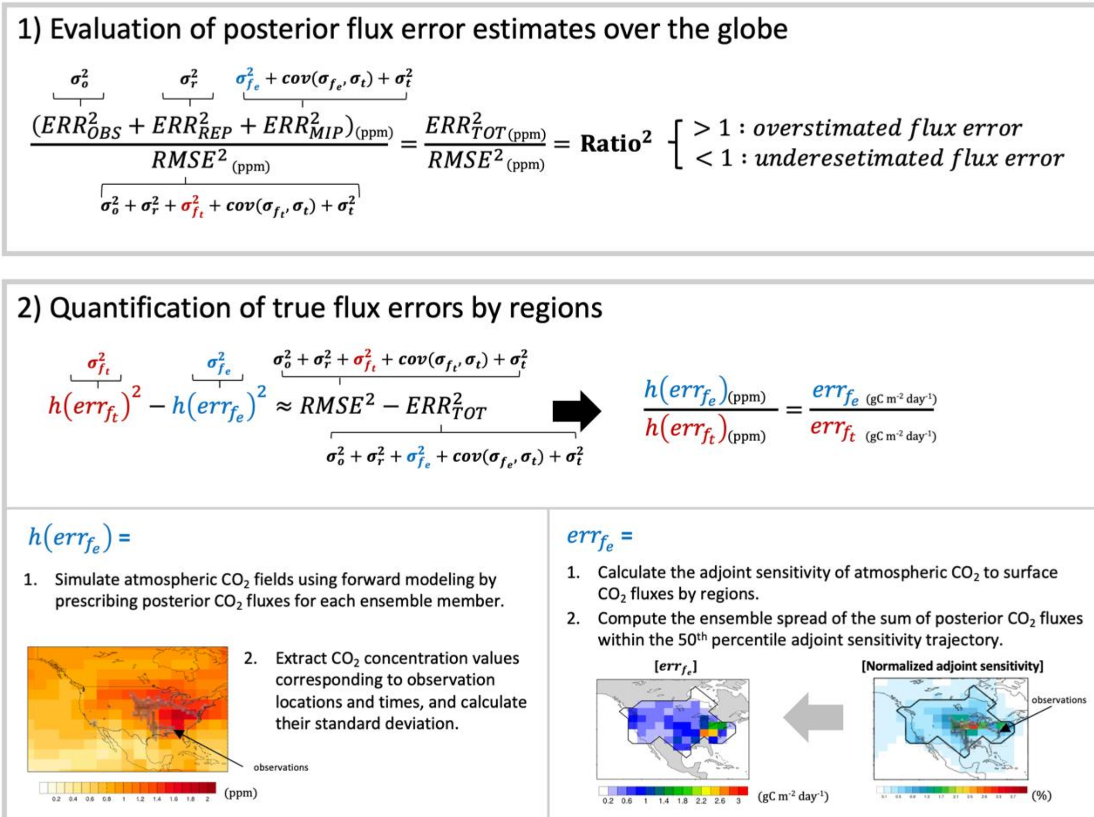

Figure 1: Flow chart summarizing the process of evaluating and quantifying errors in ensemble mean of regional posterior fluxes. RMSE² is the mean square errors between the ensemble mean of posterior CO_2 concentrations and observed CO_2 concentrations. ERR^2_{REP} and ERR^2_{OBS} denote estimates of observation errors and representation errors, respectively. ERR^2_{MIP} is an ensemble spread of posterior CO_2 concentrations. ERR^2_{TOT} is defined as the sum of ERR^2_{REP}, ERR^2_{OBS}, and ERR^2_{MIP}. err_{f_e} and err_{f_t} are estimates of flux errors, defined as an ensemble spread of posterior fluxes, and their true values. $h(err_{f_e})$ and $h(err_{f_t})$ are estimates of flux errors projected onto CO_2 concentrations and their true values. σ^2_o, σ^2_r, $\sigma^2_{f_t}$ ($\sigma^2_{f_e}$), σ^2_t, and $cov(\sigma_{f_t}, \sigma_t)$ indicate the types of errors represented by the error statics, namely observation errors, representation errors, true (estimated) flux errors projected onto CO_2 concentration, transport errors, and error covariances between the preceding two terms, respectively.

2.1 v10 OCO-2 MIP datasets

The v10 OCO-2 MIP provides multiple results from inverse models that assimilate different combinations of atmospheric CO_2 measurements for 2015–2020. Our study focused on the results from "LNLGIS" experiment, which assimilates the most observations except OCO-2 ocean glint XCO_2 retrievals that cause significant biases on inversion results (Byrne et al., 2023). The “LNLGIS” experiment incorporates v10 OCO-2 land nadir (LN) and glint (LG) XCO_2 retrievals, along with global in situ (IS) data (including surface, ship-based, and airborne measurements) included in the obspack_co2_1_OCO2MIP_v3.2.1_2021-09-14. Ten different inverse modeling groups provided monthly posterior flux estimates interpolated to 1~~°x1~~°×1° horizontal resolution and co-sampled posterior atmospheric CO_2 data at the time and location of all types of observations. All of the inversion groups used the same fossil fuel emission dataset, but they independently chose their transport models, assimilation techniques, and prior flux estimates. These details are provided in Table S1, and more detailed explanations for each inverse modeling approach can be found in Byrne et al. (2023). Although the OCO-2 MIP provides data for the period 2015–2020, we ~~used~~use data for the first three years due to the limited number of airborne measurements available during the later years. To minimize the influence of local sources and maximize the influence of regional fluxes, we ~~excluded~~exclude surface measurements and only ~~considered~~consider airborne measurements made between 1 and 5 km ~~altitude.~~ AGL. In addition, only airborne measurement data that were not assimilated in the LNLGIS experiment are used for analysis.

2.2 Airborne CO_2 measurement data

Figure 2a shows the spatial distribution of the total number of airborne ~~observations~~ CO_2 measurements used in this study ~~on a~~within each 1°x1° grid cell. The dataset includes two airborne measurement campaigns over the ocean (Atmospheric Tomography Mission; ATom; Thompson et al. 2022 and O_2/N_2 Ratio and CO_2 Airborne Southern Ocean Study; ORCAS~~) over the ocean,~~; Stephens et al. 2018), as well as ~~19~~18 campaigns over land. Specific airborne campaigns and their references are elaborated in Table 1. The majority of the datasets used in the study ~~were~~are from North America, accounting for 37~~%,~~% of the total number of observations for the period of 2015-2017, followed by East Asia with 35% and Alaska with 7~~% for the period of 2015–2017.~~%. The duration and extent of the airborne observations vary across different regions~~.~~ and time periods. Figure 2b illustrates the number of 1°×1° grid points in each of the seven regions where more than 10 observations ~~per month were~~are available per month. For Alaska, observations were concentrated during the Arctic-Boreal Vulnerability Experiment (ABoVE) campaign in 2017~~.~~ (Sweeney et al. 2022). North America had observations for most of the analysis period, ~~but observation data was collected over a wider area during~~including observations from the Atmospheric Carbon and Transport – America (ACT–America) campaign~~. In Europe, sparse observation data was made after intensive observations through the Civil Aircraft for~~ covering the ~~Regular Investigation of the atmosphere Based on an Instrument Container (IAGOS-CARIBIC) campaign in 2015.~~eastern United States (Davis et al., 2021). The Long-term Comprehensive Observation Network for TRace gases by AIrLiner (CONTRAIL; Machida et al., 2008) project provides sparse observation in Europe and continuous observation ~~data~~ in East and Southeast Asia from 2015 to 2017, as well as for Australia during 2015–2016. In South America, ~~the largest area of information was obtained when~~ measurements were conducted at six different sites in 2017: the majority of these observations come from five flask measurement sites provided by the National Institute for Space Research (INPE), which likely have a low bias in measured flask sample CO_2 mole fractions of ~1 ppm or greater when ambient water vapor mole fractions are above ~1.5%. These biases in some aircraft flask CO_2 measurements have been noted in previous literature (Baier et al., 2020; Gatti et al., 2023) and impacted data have been removed from all other aircraft flask datasets. Despite the potential limitation of these South American observations, our analysis, aimed at introducing a method for quantifying flux errors, incorporates these data to offer guidance for future studies leveraging bias-corrected observations from this region. As discussed in more detail below, readers should keep in mind that our results from South America may have lower reliability compared to those from other regions.

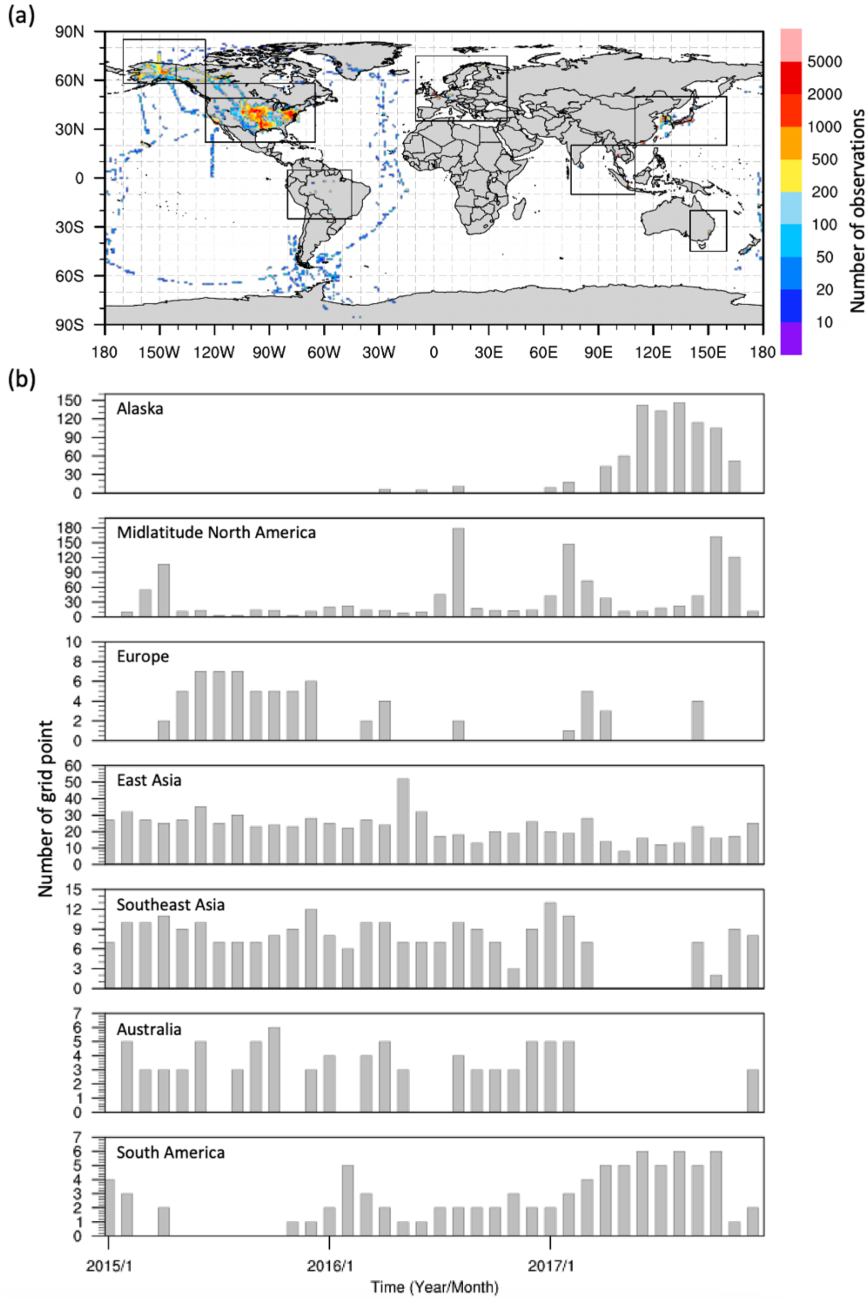

Figure 2: (a) Total number of airborne ~~measurements~~measurement data used in this study at each 1°×1° grid point and ~~monthly variations in~~(b) the number of 1~~°x1~~°×1° grid-points, where ~~observations were made for each region.~~more than 10 data is available, within each region and each month for the period 2015–2017.

Table 1. Data description for each airborne measurement campaign.

Site code	Site name	Measurement campaign name	Measurement type	Data provider	ObsPack *(original)* dataset identifier	Reference
ACG	Alaska Coast Guard, Alaska, USA	NOAA/GML Aircraft Program	In situ	National Oceanic and Atmospheric Administration (NOAA) Global Monitoring Laboratory (GML)	http://doi.org/10.25925/20201204[a]	Karion et al. (2013)
ACT	Atmospheric Carbon and Transport – America (ACT-America~~)~~), USA	ACT-America	In situ and flask	~~NASA~~National Aeronautics and Space Administration Langley Research Center (NASA-LaRC), NOAA/GML	http://doi.org/10.25925/20201204~~https://doi.org/10.3334/ORNLDAAC/1593~~[a] *https://doi.org/10.3334/ORNLDAAC/1593*	Baier et al. (2020) DiGangi et al. (2021) Wei et al. (2021)
AirCore NOAA	NOAA AirCore Program	NOAA AirCore Program	Balloon air sampler	NOAA/GML	No Obspack DOI[b] *https://doi.org/10.15138/6AV0-MY81*	Karion et al. (2010)
ALF	Alta Floresta, Brazil		Flask	National Institute for Space Research (INPE)	http://dx.doi.org/10.25925/20181030[c] https://doi.org/10.1594/PANGAEA.926834 ~~https://doi.org/10.1594/PANGAEA.949643~~	Gatti et al. (2023)
~~AOA~~CAR	~~Aircraft Observation of Atmospheric trace gases by JMA~~Briggsdale, Colorado		Flask	~~Japan Meteorological Agency (JMA)~~NOAA/GML	http://doi.org/10.25925/20210517[d]	~~Tsuboi~~Sweeney et al. (~~2013~~2015)
CON	Comprehensive Observation Network for TRace gases by AIrLiner (CONTRAIL)		In situ ~~and flask~~	National Institute for Environmental Studies (NIES), Meteorological Research Institute (MRI)	http://doi.org/10.25925/20201204~~https://doi.org/10.17595/20190828.001 https://doi.org/10.17595/20190828.002 https://doi.org/10.17595/20180208.001~~[a] *https://doi.org/10.17595/20180208.001*	Machida et al. (2008) ~~https://www.cger.nies.go.jp/contrail/index.html~~
CRV	Carbon in Arctic Reservoirs Vulnerability Experiment (CARVE~~)~~), Alaska	Arctic-Boreal Vulnerability Experiment (ABoVE)	In situ	NOAA/GML	http://doi.org/10.25925/20201204~~https://doi.org/10.3334/ORNLDAAC/1582~~[a] *https://doi.org/10.3334/ORNLDAAC/1582*	Sweeney et al. (2022)
~~DND~~GSFC	~~Dahlen, North Dakota~~Active Sensing of CO_2 Emissions over Nights, Days and Seasons (ASCENDS), USA	ASCENDS	~~Flask~~In situ	~~NOAA/GML~~NASA Goddard Space Flight Center (NASA-GSFC)	http://doi.org/10.25925/20201204[a]	~~Sweeney~~Kawa et al. (~~2015~~2018)
~~GSFC~~IAGOS	~~NASA Goddard Space Flight Center~~In-service Aircraft ~~Campaign~~for a Global Observing System	Civil Aircraft for the Regular Investigation of the atmosphere Based on an Instrument Container (IAGOS-CARIBIC)	In situ	~~NASA Goddard Space Flight Center (NASA-GSFC)~~Karlsruhe Institute of Technology (IMK-ASF), Institute for Atmospheric and Environmental Sciences (IAU), Max Planck Institute for Biogeochemistry (MPI-BGC)	http://doi.org/10.25925/20201204[a]	~~Kawa~~Filges et al. (~~2018)~~2015)
~~IAGOS~~KORUS	~~In-service Aircraft for a Global Observing System~~The Korea-United States Air	~~Civil Aircraft for the Regular Investigation of the atmosphere Based on an Instrument Container~~	In situ ~~and flask~~	~~Karlsruhe Institute of Technology (IMK-ASF), Institute for Atmospheric and Environmental Sciences (IAU), Max Planck~~	http://doi.org/10.25925/20201204[a] *https://doi.org/10.5067/ASDC/SUBORBITAL/KORUSAQ_TraceGas_AircraftInSitu_DC8_Data_1*	~~Filges~~Vay et al. ~~(2015) https://www.caribic-~~

	Quality (KORUS-AQ) field study	~~(IAGOS-CARIBIC)~~		~~Institute for Biogeochemistry (MPI-BGC)~~NASA-LaRC		~~atmospheric.com/~~., (2009)
~~LARC~~ MAN	~~LARC - NASA Langley Research Center Aircraft Campaign~~Manaus, Brazil	~~Korea-United States Air Quality Study~~NOAA/GML Aircraft Program	In situ	~~NASA-LaRC~~NOAA/GML	https://doi.org/10.25925/20210519[e]	
~~MAN~~ORC	~~Manaus~~O2/N2 Ratio and CO2 Airborne Southern Ocean Study (ORCAS)		In situ	~~NOAA/GML~~National Center for Atmospheric Research (NCAR)	http://doi.org/10.25925/20201204[a] *https://doi.org/10.5065/D6SB445X*	Stephens et al. (2018)
~~MRC~~PAN	~~Marcellus Pennsylvania~~Pantanal, Mato Grosso do Sul, Brazil		Flask	~~NOAA/GML~~INPE	http://dx.doi.org/10.25925/20181030[c]	~~Barkley et al. (2017)~~
~~ORC~~PFA	~~O2/N2 Ratio and CO2 Airborne Southern Ocean Study (ORCAS)~~Poker Flat, Alaska	NOAA/GML Aircraft Program	~~In situ~~Flask	~~National Center for Atmospheric Research (NCAR)~~NOAA/GML	http://doi.org/10.25925/20210517[d] ~~https://doi.org/10.5065/D6SB445X~~	~~Stephens~~Sweeney et al. (~~2018~~2015)
~~PAN~~RBA-B	~~Pantanal, Mato Grosso do Sul~~Rio Branco, Brazil		Flask	INPE	http://dx.doi.org/10.25925/20181030[c] *https://doi.org/10.1594/PANGAEA.926834*	Gatti et al. (2023)
~~RBA-B~~SAN	~~Rio Branco~~Santarém, Brazil		Flask	INPE	http://dx.doi.org/10.25925/20181030[c] *https://doi.org/10.1594/PANGAEA.926834* ~~https://doi.org/10.1594/PANGAEA.949643~~	Gatti et al. (2023)
~~SAN~~SGP	~~Santarem~~Southern Great Plains, Oklahoma, USA	NOAA/GML Aircraft Program	Flask	~~INPE~~The US Department of Energy (DOE)/Lawrence Berkeley National Laboratory (LBNL), NOAA/GML	http://doi.org/10.25925/20210517[d] ~~https://doi.org/10.1594/PANGAEA.949643~~	~~Gatti~~Biraud et al. (~~2023~~(2013) Sweeney et al. (2015))
SONGNEX2015	Shale Oil and Natural Gas Nexus 2015 (air campaign~~)~~), USA	Shale Oil and Natural Gas Nexus 2015 (air campaign)	In situ	NOAA Chemical Sciences Laboratory (CSL)	http://doi.org/10.25925/20201204[a]	
TEF	~~Tefe~~Tefé, Brazil		Flask	INPE	http://dx.doi.org/10.25925/20181030[c] *https://doi.org/10.1594/PANGAEA.926834* ~~https://doi.org/10.1594/PANGAEA.949643~~	Gatti et al. (2023)
TOM	Atmospheric Tomography Mission (ATom)	Atmospheric Tomography Mission (ATom)	In situ	NOAA/GML, Harvard University	http://doi.org/10.25925/20201204~~https://doi.org/10.3334/ORNLDAAC/1581~~[a] *https://doi.org/10.3334/ORNLDAAC/1581*	Thompson et al. (2022)

[a]: obspack_co2_1_GLOBALVIEWplus_v6.1_2021-03-01 (Schuldt et al., 2021b)
[b]: obspack_co2_1_AirCore_v4.0_2020-12-28
[c]: obspack_co2_1_INPE_RESTRICTED_v2.0_2018-11-13 (NOAA Carbon Cycle Group ObsPack Team, 2018)
[d]: obspack_co2_1_NRT_v6.1.1_2021-05-17 (Schuldt et al., 2021a)
[e]: obspack_multi-species_1_manaus_profiles_v1.0_2021-05-20 (Miller et al., 2021)

2.~~2~~3 Evaluation of ensemble posterior fluxes

We first ~~employed~~employ the two matrixes defined in Eq. (1) and (2) below to evaluate ensemble posterior flux errors proposed by Liu et al. (2021). One is RMSE between the ensemble mean of ~~simulated~~posterior atmospheric CO_2 from OCO-2 MIP models and the ~~observed one~~atmospheric CO_2 from airborne measurements, which can be written as:

$$RMSE^2 = \frac{1}{N}\sum_{i=1}^{N}\left[\overline{h_\iota(\hat{x})} - y_{o,i}\right]\left[\overline{h_\iota(\hat{x})} - y_{o,i}\right]^T, \text{ where } \overline{h_\iota(\hat{x})} = \frac{1}{M}\sum_{j=1}^{M} h_{i,j}(\hat{x}_j) \quad (1)$$

$\overline{h_\iota(\hat{x})}$ is the ensemble mean of posterior atmospheric CO_2 sampled at the time and location of the i^{th} airborne observation $y_{o,i}$, within each 1°×1° grid-cell in each month. *N* is the monthly total number of ~~airborne measurements within 1°x1°~~sampled data at each grid-cell~~ and~~. *M* is the number of ensemble members (i.e., 10). A single monthly *RMSE* value is computed using *N* measurement data at each grid-cell. The number of *RMSE* values is calculated per month within each region corresponds to the number of grid-cells shown in Figure 2b. The *RMSE* indicates the magnitude of the actual CO_2 errors in the ensemble estimates, which is also a quantity broadly used to evaluate the accuracy of posterior fluxes (Crowell et al., 2019; Peiro et al., ~~2021~~2022; Byrne et al., 2023). ~~However,~~ As illustrated in Figure 1 and ~~shown by Liu et al. (2021~~as described in Appendix A (Eq. A3), $RMSE^2$ includes not only the projection of true flux errors on CO_2 concentration (σ_{ft}^2), but also transport errors (σ_t^2), their error covariances ~~between the preceding two terms~~ ($cov(\sigma_{f_t},\sigma_t)$), representation errors (σ_r^2), and airborne observation errors (σ_o^2~~) including representation~~). Both transport errors and ~~measurement~~representation errors~~. Different~~ stem from ~~Liu et al. (2021), $\overline{h_\iota(\hat{x})}$ is the ensemble mean generated by multiple types of~~ transport models. Transport errors include the errors in ~~OCO-2 MIP, accounting for transport errors from~~ model structures and meteorological ~~forcing and dynamics. Note, in our analysis, outliers with more than 20 ppm differences between observation~~fields, while representation errors arise from a mismatch in resolution between model simulations and ~~model estimates were excluded from the analysis to obtain robust error estimates.~~observations.

In practice, the true flux errors are often approximated by the spread of ensemble fluxes, so the projection of true flux errors to CO_2 concentrations and transport errors are approximated by the ensemble spread of the simulated CO_2 concentrations in OCO-2 MIP as shown in Appendix A. To evaluate whether this approximation represents the true errors in the ensemble mean fluxes and mean simulated CO_2 concentrations, we define another quantity ERR_{TOT}^2 (Figure 1). Different from *RMSE*, the variance terms of flux ~~error~~errors (σ_{fe}^2) and transport ~~error~~errors (σ_t^2) and covariance terms between them ($cov(\sigma_{fe},\sigma_t)$) are replaced by the spread of ensemble (i.e., variance) posterior atmospheric CO_2 concentrations (ERR_{MIP}^2) defined as:

$$ERR_{MIP}^2 = \frac{1}{N}\sum_{i=1}^{N}\frac{1}{M}\sum_{j=1}^{M}\left[h_{i,j}(\hat{x}_j) - \overline{h_\iota(\hat{x})}\right]\left[h_{i,j}(\hat{x}_j) - \overline{h_\iota(\hat{x})}\right]^T \quad (2)$$

~~In addition,~~ Different from Liu et al. (2021) which used only one transport model, ERR^2_{MIP} accounts transport errors because posterior atmospheric CO_2 were generated by multiple types of transport models in OCO-2 MIP driven by different meteorology fields. Thus, ERR^2_{MIP} term accounts for transport errors, but not representation errors due to the coarse spatial resolution of these transport models with the highest spatial resolution being 2°×2.5°.

To obtain ~~error information~~representation errors and observation errors not captured by ERR^2_{MIP}, we additionally ~~calculated~~ calculate ERR^2_{REP} and ERR^2_{obs} ~~by combining representation error and measurement error:~~

~~$ERR^2_{obs} = ERR^2_{o\_r} + ERR^2_{o\_m}$ (3)~~

~~It corresponds to the σ_o^2 included in RMSE~~, respectively. ~~$ERR^2_{o\_r}$~~ ERR^2_{REP} indicates the representation ~~error~~errors (σ_r^2) in *RMSE²* as shown in Figure 1 and is defined as ~~within~~ a spatial variability of atmospheric CO_2 within a 2°×2.5° grid cell ~~variances of estimated atmospheric CO_2 in the models~~ written as:

$$\cancel{ERR^2_{o\_r}} = ERR^2_{REP} = \frac{1}{N}\sum_{i=1}^{N} VAR_{CO_2,i} \quad (~~4~~3)$$

~~Using~~With the high-resolution (0.5°x0.625°) 3-hourly GEOS-~~Chem~~5 simulation results for 2018 from NASA Goddard Space Flight Center (Weir et al., 2021), we ~~calculated~~calculate the ~~variances~~variance of atmospheric CO_2 concentration within each 2~~°x2~~°×2.5° grid cell at ~~a resolution of 0.5°x0.625° and sampled the values at the corresponding i^{th} airborne measurement times and locations~~every 3-hour interval. Then, we sample the CO_2 variance value ($VAR_{CO_2,i}$~~).~~) at the grid cell containing the i[th] observation and the time closest to the observation. Subsequently, the monthly mean values of the N co-sampled variances are derived~~. It is assumed~~ (ERR^2_{REP}). We assume that the variances do not vary significantly across years~~.~~, given relatively lower monthly variability of ERR_{REP} compared to that of RMSE and ERR_{MIP} (to be shown in Section 3.2). The reason for ~~choosing the 2°x2.5°, which~~ calculating CO_2 variance value within 2°×2.5° is because it is the finest resolution among the OCO-2 MIP ~~members used, is that ERR_{MIP} contains information about the difference in representation errors within the ensemble members. $ERR^2_{o\_m}$ is the observation measurement error~~models. We evaluate whether the representation errors, derived from simulated atmospheric CO_2 fields, represent the actual spatial variability of CO_2 concentration by comparing simulated CO_2 variance with the spatial variance of aircraft measurement data from ACT-America project (Supplement Text and Fig. S1). The evaluation results support our approach.

ERR^2_{OBS} represents the observation errors (σ_o^2) in *RMSE²* as shown in Figure 1. Unfortunately, this information is missing from many of the airborne measurement datasets included in the given OCO-2 MIP ObsPack format, even though uncertainties may be included in the original datasets ~~(e.g., 0.06 ppm for ACT-America; Baier et al., 2020).~~. The World Meteorological Organization (WMO) community has established network compatibility objectives for the precision of atmospheric CO_2 measurements: 0.1 ppm in the Northern Hemisphere and 0.05 ppm in the Southern Hemisphere. Assuming an ideal situation without systematic bias, we set the ~~measurement~~observation error (~~$ERR^2_{o\_m}$~~ERR_{OBS}) for all airborne observations at 0.1 ppm. However, in reality, systematic errors could be present in airborne observation ~~data~~ stemming from instrument or setup biases, calibration offsets, and other factors. Especially, CO_2 measurements in South America from INPE might exhibit a higher measurement error compared to other regions because of unresolved water vapor contamination issues in those flask measurements, which could result in both a low bias (~1-3 ppm at 3% absolute humidity, respectively) and spurious variability (Baier et al., 2020). The potential effects of these systematic errors on our findings will be addressed in Section 4. This study only employs ERR_{OBS}^2 for calculating ERR_{TOT}^2 and does not compare it with other error quantities in Section 3.

Therefore, ERR_{TOT}, the approximation for *RMSE*, is defined as:

$$ERR_{TOT}^2 = ERR_{OBS}^2 + \cancel{ERR_{MIP}^2} ERR_{REP}^2 + ERR_{MIP}^2 \qquad (\cancel{5}4)$$

By applying 1000 bootstrap resampling to the monthly grid-based error statistics (e.g., *RMSE*, ERR_{MIP}, ERR_{REP}, and ERR_{TOT}) within each region, we obtain regional mean values of these error statistics, along with their corresponding 95% confidence intervals.

To evaluate whether the spread of ensemble CO_2 fluxes from OCO-2 MIP represents the true flux errors in the ensemble mean, we ~~calculated~~calculate the ratio between monthly ~~RMSE and~~ ERR_{TOT} and *RMSE*:

$$Ratio^2 = \frac{ERR_{TOT}^2}{RMSE^2}, \qquad (\cancel{6}5)$$

~~If we could assume that~~Given that ERR_{REP}^2 reasonably depict actual representation errors, $Ratio^2$ can indicate whether posterior flux and transport errors computed from the ensemble spread is an overestimation or underestimation of true flux and transport errors. In this study, we assume that the estimated transport errors from the ensemble spread among transport models used in OCO-2 MIP represent the true transport errors and the difference between $RMSE^2$ and ERR_{TOT}^2 mainly arises from the difference in the flux error variances ($\sigma_{f_t}^2$ and $\cancel{\sigma_{fe}^2}$~~), the ratio can tell us whether the estimated posterior flux errors computed from ensemble spread is an overestimation or underestimation of true errors in the ensemble mean.~~$\sigma_{f_e}^2$). Thus, a ratio close to 1 indicates that the estimated posterior flux errors derived from the ensemble model spread are close to the true posterior flux error in the ensemble mean fluxes. A ratio greater than 1 means that the posterior flux errors are overestimated, and vice versa. ~~Finally, by applying 1000 bootstrap resampling to the monthly grid-based matrices for each region, the regional average of error matrices is obtained, along with its corresponding 95% confidence intervals~~However, our assumption regarding transport errors may be a strong assumption given that the transport errors are derived from 10 ensemble members, covering four different transport models, which might not fully capture the actual transport errors. We discuss how this assumption affects our key results in Section 4.

2.~~3~~4 Quantification of the uncertainties of ensemble mean of posterior fluxes

In addition to the qualitative evaluations of posterior flux errors using the ratios between ~~RMSE and~~ ERR_{TOT} and RMSE, we propose a method to quantitatively assess the ensemble posterior flux errors (i.e., variance of flux errors) in both CO_2 space and flux space. To do this, we first need to calculate the variance of atmospheric CO_2 errors due to only the ensemble spread of posterior fluxes from OCO-2 MIP ($h(err_{f_e})^2$). As shown in the Appendix A, this term can be written as:

$$h(err_{f_e})^2 \cancel{= \frac{1}{N}} = \frac{1}{N}\sum_{i=1}^{N}\frac{1}{M}\sum_{k=1}^{M}\frac{1}{M}\sum_{j=1}^{M}\left[h_k(\hat{x}_{k,i}) - h_k(\hat{x}_{j,i})\right]\left[h_k(\hat{x}_{k,i}) - h_k(\hat{x}_{j,i})\right]^T$$

(~~7~~6)

Using all transport models engaged in the OCO-2 MIP would be ideal to derive $h(err_{f_e})^2$, but, in this study, we ~~approximated~~approximate this error term using the GEOS-Chem model as depicted:

$$h(err_{f_e})^2 \approx h_{GC}(err_{f_e})^2 = \frac{1}{N}\sum_{i=1}^{N}\frac{1}{M}\sum_{j=1}^{M}\left[\overline{h_{GC}(\hat{x}_i)} - h_{GC}(\hat{x}_{j,i})\right]\left[\overline{h_{GC}(\hat{x}_i)} - h_{GC}(\hat{x}_{j,i})\right]^T, \qquad (~~8~~7)$$

where $\overline{h_{GC}(\hat{x}_i)} = \frac{1}{M}\sum_{j=1}^{M} h_{GC}(\hat{x}_{j,i})$

To get $h_{GC}(err_{f_e})^2$, we ~~conducted~~conduct a set of forward simulations using the GEOS-Chem transport model (within the GEOS-Chem Adjoint model ~~(~~v8.2j; Henze et al., 2007). In all ten experiments, consistent meteorology and emission forcing data ~~were~~are used from the Modern-Era Retrospective analysis for Research and Applications version 2 (MERRA-2; Gelaro et al., 2017~~),~~) and Open-source Data Inventory for Anthropogenic CO_2 (ODIAC; Oda and Maksyutov, 2015~~), and Global Fire Emissions Database version 4 (GFEDv4; Randerson et al., 2015~~); identical annually balanced ~~3-~~hourly terrestrial biosphere fluxes from ~~SiB3 (Baker~~SiB4 (Haynes et al., ~~2010~~2021) were also employed. However, in each experiment, the prescribed monthly fluxes of terrestrial ecosystems and oceans ~~were~~are based on the posterior fluxes from the respective ten OCO-2 MIP ensemble members. All experiments ~~were~~are performed at 2~~°x2~~°×2.5° horizontal resolution and 47 vertical levels for the period 2015–2017. By calculating the mean of variances of simulated CO_2 concentrations among the ten experiments at i^{th} airborne observations within each 1~~°x1~~°×1° grid-cell, we ~~derived the~~derive $h_{GC}(err_{f_e})^2$.

Because we assume that the spread of ensemble transport models used in OCO-2 MIP represents the true transport errors included in *RMSE*^{2}, the transport errors along with observation errors and representation errors would cancel out when we calculate the difference between monthly *RMSE*^{2} and ERR_{TOT}^2 ~~mainly~~. Consequently, the difference between monthly *RMSE*^{2} and ERR_{TOT}^2 arises from the difference in the flux error variances ($\sigma_{f_t}^2$ *and* $\sigma_{f_e}^2$~~),~~). The difference between monthly true flux errors ($h(err_{f_t})^2$) and estimated flux errors ($h(err_{f_e})^2 \approx h_{GC}(err_{f_e})^2$) projected onto CO_2 space can be derived from the difference between *RMSE*^{2} and ERR_{TOT}^2 as shown:

$$h(err_{f_t})^2 - h(err_{f_e})^2 = RMSE^2 - ERR_{TOT}^2 \qquad (~~9~~8)$$

From Eq. (~~9~~8), we can derive the true errors of the ensemble mean fluxes in CO_2 space, $h\left(err_{f_t}\right)^2$. Out of 181 cases, representing the total months of observations across all seven regions, $h\left(err_{f_t}\right)$ can be derived using this equation in 158 cases. In 23 cases (13% of total cases), $h\left(err_{f_t}\right)$ cannot be derived when ERR_{TOT} and/or $h\left(err_{f_e}\right)$ values fell outside the applicable range. Around 40% of the exception cases occur in South America where observation cover only one to six 1°×1° grid cells per month, suggesting that observations are insufficient to quantify the monthly flux errors in this region.

In order to link ~~this term~~those terms with flux errors in flux space, we first identify the areas ~~that these CO_2 concentrations are~~ sensitive to airborne CO_2 measurements by conducting sensitivity experiments using the GEOS-Chem Adjoint model. Seven sets of adjoint sensitivity experiments are conducted to examine the sensitivity of airborne measurements in each region (defined in Figure 2a) to terrestrial biosphere and ~~ocean~~air-sea CO_2 fluxes for the month of ~~observation~~observations. The sensitivity experiments ~~used~~use the same meteorology and CO_2 emission datasets as the forward simulations, along with the ensemble mean of posterior terrestrial biosphere and air-sea flux values. The following explanation of the sensitivity analysis uses the same notation as Liu et al. (2015). The cost function (J) is defined as the sum of simulated CO_2 concentrations where airborne observations were made within each region and month:

$$J = \sum_{i=1}^{N} h_i(\hat{x}), \qquad (\cancel{10}9)$$

The sensitivity of observations to surface fluxes at l^{th} grid-cell and t^{th} time is derived from the partial derivative of J with respect to surface fluxes ($\hat{x}_{l,k}$) written as:

$$\gamma_{l,t} = \frac{\partial J}{\partial \hat{x}_{l,t}}, \qquad (\cancel{11}10)$$

Monthly cumulative sensitivity (β) with respect to surface fluxes is determined by integrating $\gamma_{l,t}$ from the measurement time (t_0) to the initial time (t_{-T}) for each month:

$$\beta_l = \sum_{t=t_0}^{t_{-T}} \gamma_{l,t}, \qquad (\cancel{12}11)$$

In order to find the most sensitive areas to the ~~observation~~airborne observations, we ~~selected~~select the areas accounting for 50% of the global total values of β~~. We then calculated the estimated posterior flux errors in flux space ($err_{fe}^2 = \sigma_{fe}^2$) by calculating the ensemble spread of the average (~~ for each region and ~~sum) of posterior flux values from OCO-2 MIP within these areas. Regions~~month. Areas with sensitivity values lower than 0.1% (0.15% for Alaska, Australia, and Southeast Asia) of the total value of β ~~were~~are excluded due to occasional cases where observations ~~were~~are influenced uniformly across too wide regions as a result of active atmospheric mixing. Additionally, to avoid excessive consideration of localized effects due to a large number of observations occurring in a single location, regions with sensitivity values greater than 1% ~~were included in the effective area~~are included in the effective area. We then compute the estimated posterior flux errors in flux space ($err_{f_e}^2 = \sigma_{f_e}^2$) by calculating the ensemble spread of the total posterior flux values (and area-averaged mean values) over the effective area for each month for the period 2015–2017, as illustrated in Figure 1. The estimated mean posterior fluxes (err_{f_e}) over the selected areas in each month, exhibits a significant correlation ($p \leq 0.05$) with the monthly $h(err_{f_e})$ in all regions, except for Australia where the observational campaign was conducted in specific months (Fig. S2). While the observed atmospheric CO_2 concentration is influenced by both terrestrial biosphere and ocean sources, a comparison of the magnitudes of err_{f_e} between ocean and land within the effective areas reveals that, on average, the terrestrial biosphere flux error contributes more than 95% to the total posterior flux errors in all regions (Fig. S3). This result indicates that our evaluation results based on atmospheric CO_2 can be applied to deriving the actual errors of posterior terrestrial biosphere flux within the selected area in flux space.

This study provides both monthly and three-year mean values of regional flux error statistics for the period 2015–2017. Technically, it is possible to derive the monthly true errors in the ensemble mean of terrestrial biosphere fluxes within the effective areas using the monthly error statistics. However, to obtain more robust results, we compute the true errors of annual total terrestrial biosphere fluxes over the analysis period. To identify the areas contributing most to the computed mean error statistics, we calculate the number of months selected as the effective areas for monthly airborne observations. Those grid cells, at 2°×2.5° resolution, corresponding to the effective areas are assigned a value of 1, while the remaining cells are assigned a value of 0 for each month. We then calculate composite values for each grid cell over the three years. A higher number of months indicates more information in those grid cells was utilized in calculating the three-year regional mean error statistics. We define that our three-year mean error statistics mostly represent the areas where the composite values exceed eight, corresponding to 20% of the total analysis months (i.e., 36).

The observation operator, which converts surface fluxes to atmospheric CO_2, is generally assumed linear~~, therefore,~~. Therefore, we can obtain the true annual total terrestrial biosphere flux errors in those areas, err_{f_t} $(= \sigma_{f_t})$~~,~~ by multiplying the ratio between three-year mean values of $h(err_{f_t})$ and $h(err_{f_e})$ ~~with err_{f_e}, we obtain the true errors in~~ by the ensemble ~~mean fluxes, err_{f_t} $(= \sigma_{f_t})$.~~spread of the mean annual total terrestrial biosphere flux estimates (err_{f_e}) within the effective areas. The equation can be written as:

$$err_{f_t} = \frac{h(err_{f_t})}{h(err_{f_e})} \times err_{f_e}$$ (~~13~~12)

Lastly, to explore characteristics of regions where average annual total err_{f_t} is significantly underestimated, we also compute the average annual fossil fuel CO_2 emissions in the effective area using ODIAC data.

3 Results

3.1 Spatiotemporal variations ~~in~~of the ensemble posterior CO_2 concentration errors and other major error components

Because the magnitude of terrestrial biosphere CO_2 fluxes is generally over 10 times greater than air-sea fluxes, the observed atmospheric CO_2 over the oceans carries signals from nearby land fluxes. The four ATom campaigns spanning four seasons and the ORCAS campaign during austral summer spanned wide latitudinal ranges, primarily over the oceans, providing a unique opportunity to analyze the latitudinal distributions of inverse modeling errors and contributions of main error sources. We compare the ensemble posterior CO_2 to airborne CO_2 measurements taken between 1-5 km AGL and then calculate the mean error statistics for the entire campaign period. Comparisons to observations from ATom and ORCAS campaigns reveal a general increase in *RMSE* values towards the northern high latitudes, reaching 1.2 ppm at 40°N (Figure 3a, f). The latitudinal gradient becomes particularly evident during the summer season, with *RMSE* values exceeding ~~2~~1.5 ppm over North America (Fig. ~~S1~~S4), suggesting significant contributions of errors in ~~posterior~~ terrestrial biosphere fluxes to the differences between observed and simulated atmospheric CO_2. Additionally, consistently elevated *RMSE* values (>~~2~~1.5 ppm) commonly ~~appeared~~appear over the west coast of Africa throughout the seasons.

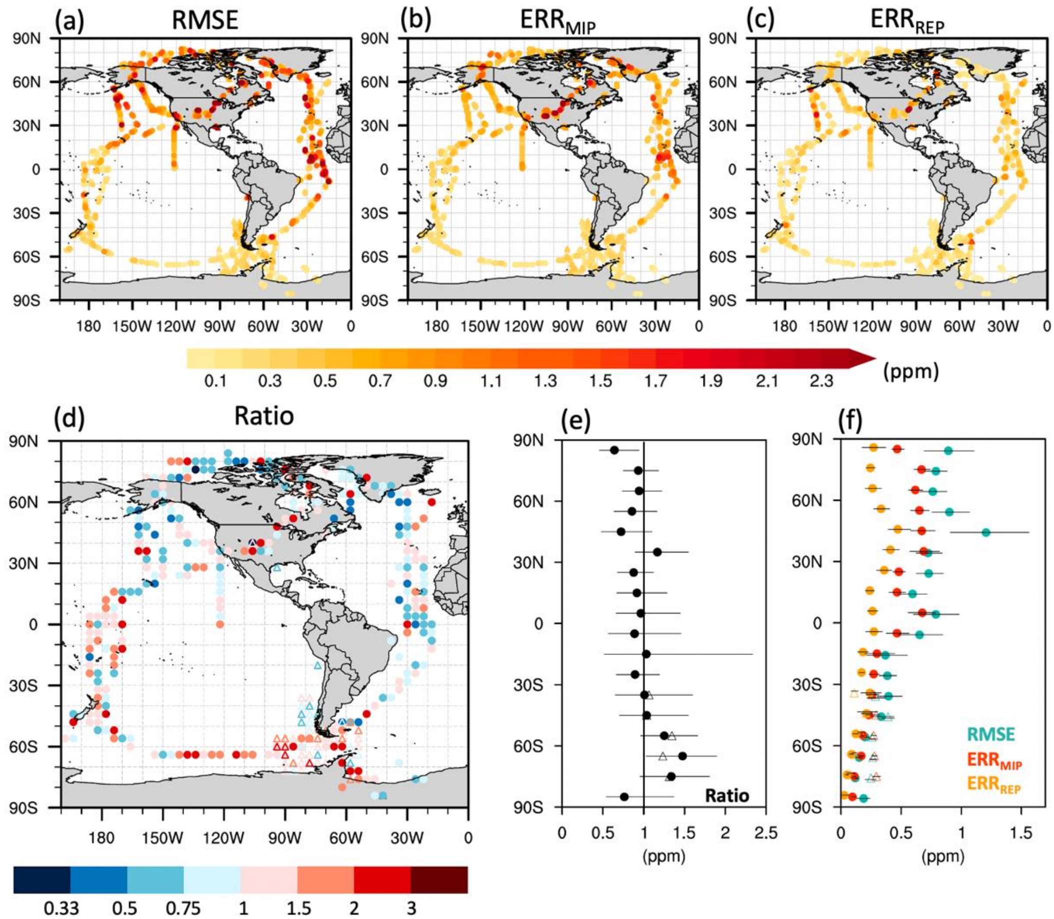

Figure 3: Spatial distributions of (a) *RMSE*, (b) *ERR_MIP*, (c) ~~ERR_OBS~~*ERR_REP*, and (d) *Ratio* (= $\cancel{\sqrt{ERR_{OBS}^2 + ERR_{MIP}^2}}\sqrt{(ERR_{OBS}\,(=0.1\,ppm))^2 + ERR_{REP}^2 + ERR_{MIP}^2}\,/\,RMSE$) where ATom (circle) and ORCAS (triangle) airborne measurements were taken and (e and f) their latitudinal distributions smoothed by 10° moving average with 95% confidence intervals derived from 1000 bootstrap samples of datasets (error bar).

Both ERR_{MIP} and ~~ERR_OBS~~ERR_{REP} exhibit similar spatial distributions as *RMSE* (Figure 3a-c, f). However, ERR_{MIP} has a stronger positive correlation with *RMSE* (r = 0.~~60~~57 and 0.~~81~~58 for ATom and ORCAS, respectively) compared to ~~ERR_OBS~~ERR_{REP} (r = 0.35 and 0.~~46~~32), with an average greater magnitude (0.~~51~~49 and 0.~~33~~32 ppm) than ~~ERR_OBS~~ERR_{REP} (0.~~37~~27 and 0.~~32~~20 ppm) globally for the whole campaign periods. Particularly, ERR_{MIP} and ~~ERR_OBS~~ERR_{REP} account for ~~67~~75% and ~~33~~37% of the anomalous high *RMSE* values (~~2.2~~1.5 ppm) in Northern America (32-50N and 85-124W), and ~~84~~75% and ~~38~~30% of the *RMSE* values (1.2 ppm) along the ~~east~~west coast of Africa. These findings indicate that ERR_{MIP} which represents errors in posterior fluxes and transport is the most significant factor in explaining *RMSE*.

Next, in order to assess the proximity of the estimated posterior flux errors, based on the spread of OCO-2 MIP ensemble fluxes, to the true posterior flux errors of the ensemble mean, we ~~compared the root mean square error (~~compare *RMSE*~~)~~ with the sum of ERR_{MIP}, ERR_{REP}, and ERR_{OBS} (referred to as ERR_{TOT}). The ratio of ERR_{TOT} to *RMSE* exceeds one over the tropical Pacific and the Southern Ocean (Figure 3d, e), indicating that the ensemble spread of posterior fluxes overestimates true flux errors over the regions sensitive to these observations. This overestimation pattern consistently appears for both the ATom and ORCAS campaigns across all seasons (Fig. ~~S2~~S5). Airborne CO_2 measurements in this area are predominantly influenced by air-sea fluxes due to the limited land extent and the significant distance from land (Yun et al., 2022), suggesting the true posterior air-sea flux errors may be smaller than the spread of the ensemble posterior flux estimates. In contrast, a ratio of ERR_{TOT} to *RMSE* less than one was observed along the African coast during the ATom campaigns, with the exception of the 2018 spring campaign conducted in a relatively distant region from Africa. Considering that these airborne observations are known to be sensitive to terrestrial biosphere fluxes in tropical Africa (Liu et al., ~~2022~~2021), our results imply that true errors of the ensemble mean terrestrial biosphere fluxes in this region may be larger than the estimated errors based on the OCO-2 MIP ensemble spread. These findings agree with Liu et al. (~~2022~~2021), which demonstrated an underestimation of posterior flux errors in CMS-Flux inverse model, ~~indicating~~suggesting most of the inverse models in OCO-2 MIP have ~~common~~ significant errors for this region.

In the northern mid-to-high latitudes, characterized by significant terrestrial CO_2 flux impacts on atmospheric CO_2 variations (Yun et al., 2022), the ratio of ERR_{TOT} to *RMSE* exhibits substantial variation across space and time. The ratio between ERR_{TOT} to *RMSE* is greater than one within the North American continent during summer and autumn. However, in other areas, there is a mixed pattern with ratios both below and above one, although the majority of the areas exhibit ratios less than one during winter. These findings highlight that the degree of underestimation or overestimation of true terrestrial biosphere flux errors based on ensemble spread can differ depending on regions and seasons, emphasizing the need for a more detailed evaluation of terrestrial biosphere flux errors at a regional level based on long-term independent observation ~~data~~.

3.2 Evaluation of v10 OCO-2 MIP ensemble posterior CO_2 flux errors by regions

In this section, we ~~calculated~~calculate the regionally averaged monthly error statistics by comparing the ensemble posterior CO_2 to airborne measurements over seven regions for 2015–2017. *RMSE* values in all these regions exhibit significant monthly variations, with ~~a~~values falling within the range of 1-3 ppm, with no clear seasonality possibly due to variations in observation routes (Figure 4). Consistent with the results shown in Section 3.1, ERR_{MIP} is the most significant factor explaining the variations of *RMSE*. Among the seven regions, significant positive correlations ($p<0.05$) between monthly *RMSE* and ERR_{MIP} exist in Alaska (r=0.~~53~~46), mid-latitude North America (r=0.~~45~~63), Europe (r=0.~~68~~60) and East Asia (r=0.~~61~~60). Furthermore, the correlation coefficient is greater than or comparable to that with ~~ERR_{OBS}~~ERR_{REP}. This suggests that in these regions, temporal variations of the errors in posterior fluxes and transport are the major contributors to the temporal variations of *RMSE*. On the other hand, *RMSE* ~~did~~does not exhibit a significant correlation with either ERR_{MIP} or ~~ERR_{OBS}~~ERR_{REP} in Southeast Asia, Australia, and South America. This implies that the estimated posterior flux errors based on ensemble spread may not represent the temporal variations in true flux errors in those regions.

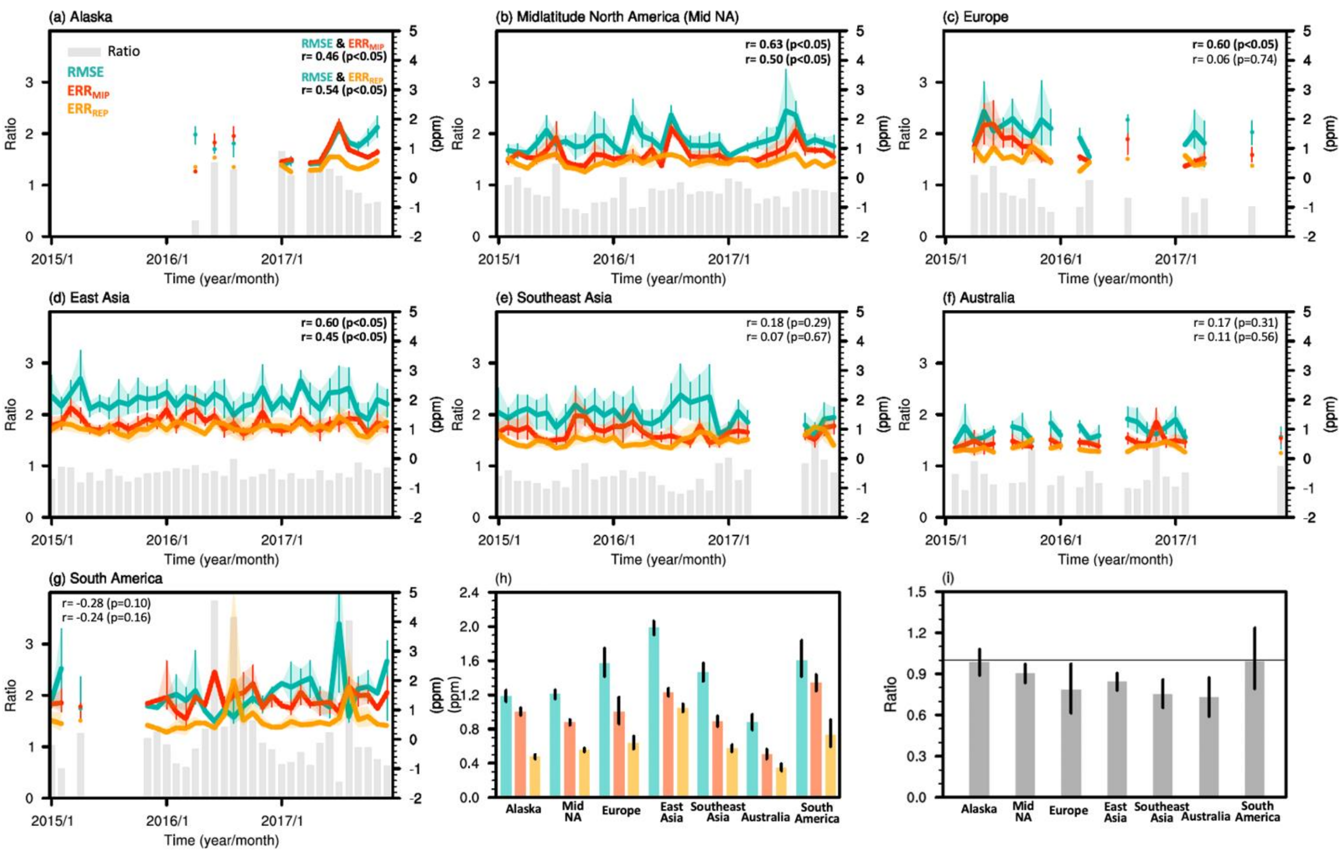

Figure 4: (a-g) Monthly ~~variations~~values of *RMSE*, ERR_{MIP}, ~~ERR_{OBS}~~ERR_{REP}, and *Ratio* for each region and (h, i) their mean values for the period 2015–2017. The upper right number in (a-g) indicates the correlation ~~coefficient~~coefficients between *RMSE* and ERR_{MIP} and ~~ERR_{OBS}~~ERR_{REP}. The shaded areas and error bars represent the 95% confidence intervals derived from 1000 bootstrap samples of datasets.

RMSE values exhibit significant variability not only over time but also across regions. The three-year average ~~monthly~~ *RMSE* is the largest in East Asia (~~2.04 [~~1.~~95~~98 [1.90, 2.~~13~~06] ppm: mean [95% confidence intervals]), followed by ~~South America (1.66 [~~Europe (1.~~46,~~57 [1.~~88~~41, 1.74] ppm) and the lowest in Australia (0.~~90~~88 [0.~~81~~79, 0.~~99~~97] ppm), followed by Alaska (1.19 [1.12, 1.~~26~~25] ppm). ERR_{MIP} is the primary error component for *RMSE*, accounting for ~~59-89~~58-83% of the *RMSE*, surpassing the ~~ERR_{OBS}~~ERR_{REP} in all the regions by 1.2-2.1 ~~times~~time. In East Asia, the difference between ERR_{MIP} and ~~ERR_{OBS}~~ERR_{REP} is relatively small compared to other regions. This could be attributed to the presence of numerous significant carbon sources, particularly along the coastal areas, resulting in increased spatial variability of CO_2 within the coarse grid cell of OCO-2 MIP inverse modeling.

The ratio between ERR_{TOT} and $RMSE$ ~~serves as an indicator of how closely the estimated errors based on the ensemble spread of OCO-2 MIP fluxes align with true errors in the ensemble mean fluxes in each region.~~also show significant variability across regions. Our results ~~show~~indicate that, on average, the estimated flux errors in Alaska and South America ~~exhibited slight overestimation of~~closely match the true flux ~~error~~errors with ratios of ~~1.04 [~~0.~~93~~98 [0.89, 1.~~14~~08] and 0.99 [0.79, 1.~~01 [0.81, 1.25~~24], respectively, while mid-latitude North America, Europe, East Asia, Southeast Asia, and Australia ~~showed~~ show significant underestimation at a 95% confidence level with ratios of 0.90 [0.83, 0.97], 0.79 [0.~~62~~61, 0.~~98~~97], 0.84 [0.78, 0.91], 0.75 [0.~~66~~65, 0.~~85~~86], and 0.~~76~~73 [0.~~61~~59, 0.~~90~~87], respectively, throughout the analysis period. ~~Moreover, we observed significant~~ Furthermore, the monthly ~~variability in the~~ variabilities (i.e., standard deviation) of the ratios ~~of ERR_{TOT} to RMSE~~are much greater in regions with diverse campaign durations and routes, such as South America~~.~~ ~~In contrast,~~ (0.87), than in East Asia~~,~~ (0.21), characterized by a consistent three-year observation campaign along the same paths~~, exhibits relatively lower variability~~. This suggests that the spatial variability in the degree of flux error underestimation or overestimation may ~~be greater than~~exceed the temporal variability.

3.3 Error quantification of v10 OCO-2 MIP ensemble posterior terrestrial biosphere CO_2 fluxes by regions

~~**Next, to quantitatively calculate the true regional posterior CO_2 flux errors, we computed monthly mean atmospheric CO_2 errors due to the estimated posterior flux errors (i.e., $h(err_{f_e})$) by conducting forward transport model simulations. The average contributions of monthly $h(err_{f_e})^2$ to ERR_{MIP}^2 are the highest in Australia (76%), followed by Alaska (65%), and lowest in Europe (34%), followed by East Asia (40%), indicating notable contributions of transport error and/or their covariances with flux error to the ERR_{MIP}^2 in the latter regions (Fig. S3).**~~Next, by incorporating the monthly *RMSE*, ERR_{TOT}, and $h(err_{f_e})$, we ~~**calculated**~~derive monthly true posterior flux ~~**error**~~errors in CO_2 space (i.e., $h(err_{f_t})$) for each region during the period 2015–2017 (Figure 5). ~~**The**~~Regionally averaged $h(err_{f_t})$ ~~**calculation was applicable in the majority of cases (159 out of 183, 87% of the total), with exceptions**~~exhibits different seasonal and monthly variability compared to $h(err_{f_e})$. In the northern mid-latitude regions, $h(err_{f_e})$ shows clear seasonal cycles for ~~**a few instances where the ERR_{TOT} or**~~the entire analysis period, despite different observation routes in each month. For example, in mid-latitude North America and East Asia, the growing season (May to October; 0.6 and 0.9 ppm, respectively) experiences higher $h(err_{f_e})$ ~~**values fell outside the applicable range, especially in**~~ than the non-growing season (November to April; 0.4 and 0.7 ppm). The seasonal variations are also observed in $h(err_{f_t})$ in East Asia and partially in mid-latitude North America for 2017, but they are not discernible in Alaska and Europe. In addition, monthly $h(err_{f_t})$ does not exhibit a significant correlation ($p<0.05$) with monthly $h(err_{f_e})$ in Alaska, midlatitude North America, Southeast Asia, and South

America. $h(err_{f_t})$ displays greater monthly variability than $h(err_{f_e})$. For example, in mid-latitude North America and East Asia, the standard deviation of monthly $h(err_{f_t})$ is 1.8 and 2.3 times greater than that of monthly $h(err_{f_e})$.

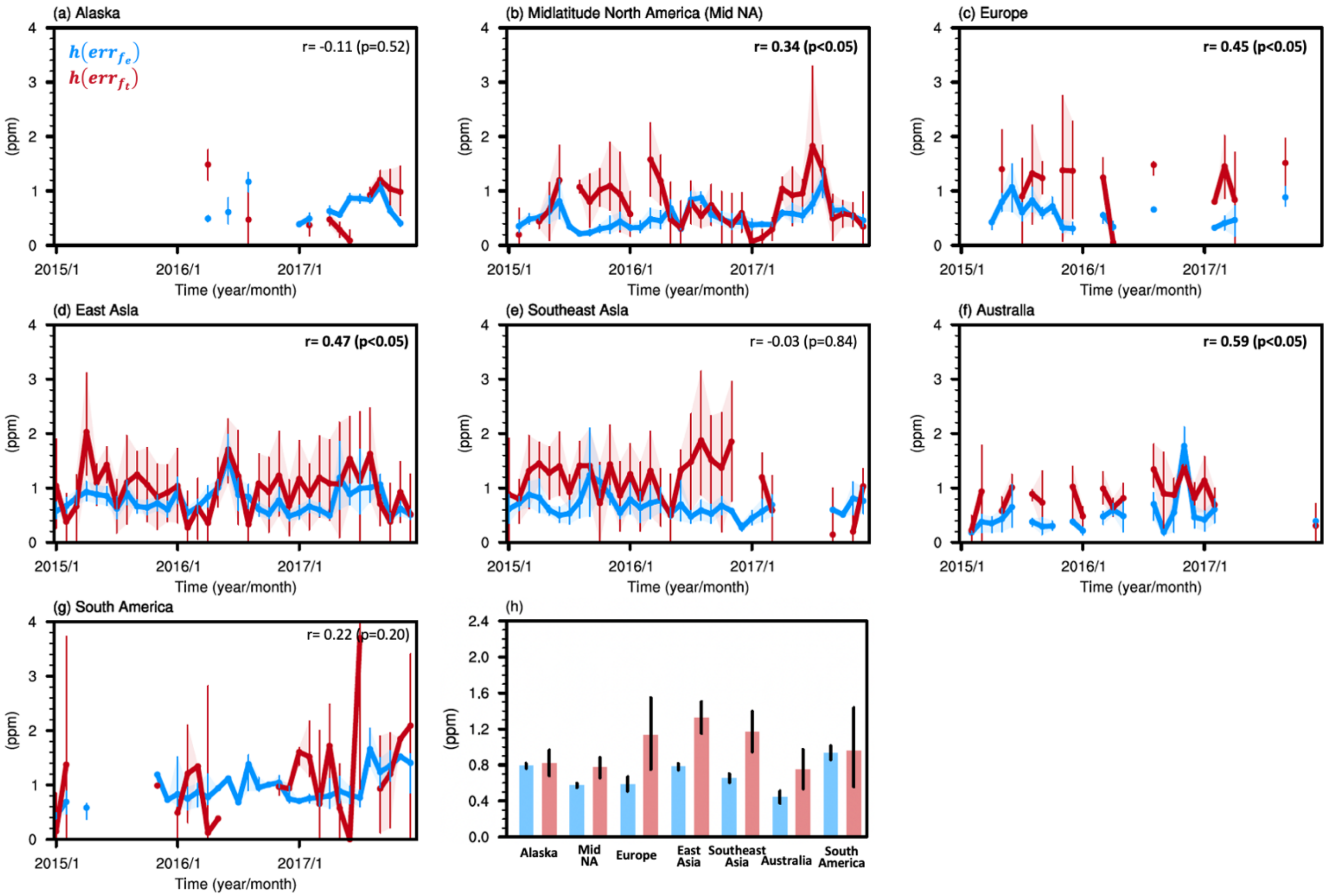

Figure 5: (a-g) Monthly ~~variations~~values of $h(err_{f_e})$ and $h(err_{f_t})$ for each region and (h) their mean values for the period 2015–2017. The upper right number indicates the correlation coefficient between them. The shaded areas and error bars represent the 95% confidence intervals derived from 1000 bootstrap samples of datasets.

~~A significant positive correlation ($p<0.05$) between the regionally averaged monthly true flux errors in CO_2-space and the estimated CO_2 errors is observed in three of seven regions (Figure 5a-g). However, the true flux errors in CO_2-space $h(err_{f_t})$ exhibit distinct patterns of variability compared to the estimated CO_2 errors, $h(err_{f_e})$. In the northern mid-latitude regions, $h(err_{f_e})$ shows clear seasonal cycles for the entire analysis period, despite different observation routes in each month. The seasonal variations are also observed in $h(err_{f_t})$ in Alaska and partially in mid-latitude North America for 2017, but they are not discernible in Europe and East Asia. For example, in East Asia, the growing season (May to October; 1.1~~

~~ppm) experiences higher $h(err_{f_e})$ than the non-growing season (November to April; 0.8 ppm), but the difference in $h(err_{f_t})$ between these seasons is only 0.1 ppm. Moreover, $h(err_{f_t})$ displays greater monthly variability than $h(err_{f_e})$. These findings suggest that while the ensemble model spread is capable of capturing general temporal variations of true posterior flux errors in some regions, it may not fully manifest its specific characteristics of seasonal and monthly variability.~~

The comparison between the three-year average $h(err_{f_t})$ and *RMSE* highlights the substantial contributions of posterior flux errors to the differences between airborne observations and simulated atmospheric CO_2 from OCO-2 MIP ensemble models. The $h(err_{f_t})$ tends to be larger in regions with higher *RMSE*, peaking in East Asia ($h(err_{f_t})$=1.32 ppm and *RMSE*=1.98 ppm) and reaching a minimum in Australia ($h(err_{f_t})$=0.75 ppm and *RMSE*=0.88 ppm) (Figures 4h and 5h). The $h(err_{f_t})$ accounts for up to 85% of the *RMSE* in Australia, followed by Southeast Asia (80%) and a minimum of 60% of the *RMSE* in South America, followed by mid-latitude North America (64%). This indicates dominant contributions of posterior flux errors to *RMSE*, surpassing representation and transport errors in the first two regions.

The regional ~~average values of the~~mean ratios between $h(err_{f_e})$ and $h(err_{f_t})$ throughout the analysis period ~~show~~ indicate significant underestimations at a 95% confidence level of true posterior flux errors in mid-latitude North America, Europe, East Asia, Southeast Asia, and Australia by a factor of 0.~~73~~74 [0.~~59~~61, 0.~~86~~88], 0.52 [0.~~29~~27, 0.~~77~~78], 0.59 [0.48, 0.70], 0.56 [0.~~42~~41, 0.~~71~~72], and 0.~~61~~59 [0.~~35~~34, 0.~~91~~87], respectively (Figure 5h). In contrast, Alaska and South America exhibit ~~a slight overestimation~~comparable estimates of true flux errors by factors of ~~1.07 [~~0.~~84~~96 [0.76, 1.~~31~~17] and ~~1.03~~0.97 [0.49, 1.~~59~~54], respectively~~, with a particularly large uncertainty range in South America.~~. The regions with significant underestimation ~~and overestimation~~ align with those identified in the previous analysis based on ratios between ERR_{TOT} and *RMSE*~~,~~ (Section 3.2), but the $h(err_{f_e})$ to $h(err_{f_t})$ ratios ~~are smaller for~~imply weaker underestimation ~~and~~ of true flux errors. The ratios have larger ~~for overestimation. The regional average of $h(err_{f_t})$ has a tendency to be larger~~uncertainty range in the regions ~~with higher RMSE values with a maximum~~where observations conducted over limited times and locations, such as those in ~~East Asia (1.36 ppm) and a minimum in~~ Europe, Australia ~~(0.75 ppm). The $h(err_{f_t})$ account for up to 84% of the RMSE in Australia and a minimum of 58% of the RMSE in~~, and South America than in the mid-latitude North America and East Asia where observations cover wider areas and ~~exceed the observation errors in all regions. The results highlight the substantial contributions of posterior flux errors to the differences between airborne observations and simulated atmospheric CO_2 from OCO-2 MIP ensemble models~~occur more frequently.

Finally, by using the three-year regional mean ratios between $h(err_{f_e})$ and $h(err_{f_t})$, we compute the true errors in the annual terrestrial biosphere fluxes over the effective areas averaged for the period 2015–2017 (Figure 6). We find that the actual terrestrial biosphere flux errors are underestimated, particularly in regions where annual CO_2 emissions from fossil fuel combustion exceed annual terrestrial biosphere fluxes by 3-31 times. The airborne measurements carried out in mid-latitude North America, East Asia, and Southeast Asia are influenced by a broad region encompassing the United States, the eastern part of East Asia, and the western part of Southeast Asia where fossil fuel CO_2 emissions are 1,341, 2,443, and 815 Tg C year^{-1}, respectively. The first two regions are estimated as significant terrestrial biosphere CO_2 sinks, with estimated fluxes of −414 ± 279 (ensemble mean ± 1σ) and −561 ± 380 Tg C year^{-1}, in contrast to Southeast Asia (26 ± 118 Tg C year^{-1}). However, the CO_2 sinks are more than 3 and 4 times smaller than the fossil fuel CO_2 emissions, respectively. The recalculated terrestrial biosphere flux errors in these regions exceed the ensemble spread with values of 374, 643, and 211 Tg C year^{-1}. Observations in Europe and Australia, conducted over limited periods and specific locations, mainly represent certain areas in the western Europe and the southeastern part of Australia, where fossil fuel emissions (234 and 53 Tg C year^{-1}, respectively) are around four and five times greater than terrestrial biosphere sinks (−51 ± 34 and −10 ± 67 Tg C year^{-1}). The recalculated terrestrial biosphere flux errors in these regions are also larger than the ensemble spread, estimated at 65 and 114 Tg C year^{-1}, respectively. On the contrary, the most influential areas for the observation in Alaska and South America, encompassing the southeastern region of Alaska and the northern part of Brazil, characterized as a terrestrial biosphere sinks of −8 ± 11 Tg C year^{-1} and sources of 625 ± 387 Tg C year^{-1}, respectively, which are comparable to or more than 10 times greater than fossil fuel emissions (10 and 38 Tg C year^{-1}). The observation-based estimates of true terrestrial biosphere flux errors are almost identical to the ensemble spread in both regions with values of 11 and 398 Tg C year^{-1}, respectively.

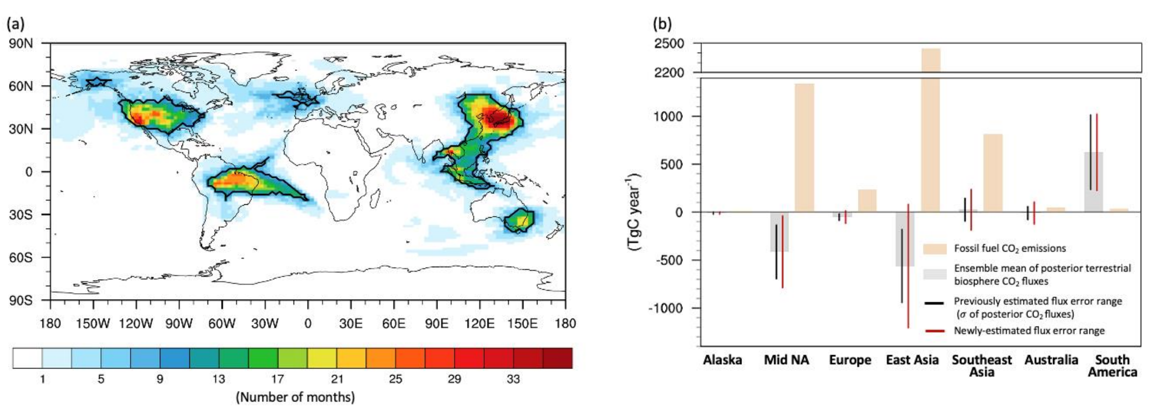

Figure 6: (a) Number of months selected as the effective area for airborne measurements. The outlined area represents selected areas for more than eight months or equal. (b) Annual total terrestrial biosphere CO_2 ~~flux~~fluxes obtained from the ensemble mean of ten ~~inversion estimates~~OCO-2 MIP models and annual total fossil fuel CO_2 emissions estimated from ODIAC data for each outlined area averaged over the period 2015–2017. The error bars in black and red indicate the one standard deviation of the inversion estimates and the newly estimated error range from this study, respectively.

~~The airborne observations carried out in mid-latitude North America and East Asia are influenced by a broad region encompassing the United States and eastern parts of East Asia, known for significant terrestrial carbon sinks with estimated~~

~~fluxes of −436 ± 277 (ensemble mean ± 1σ) and −559 ± 379 TgC year^{-1}. The recalculated terrestrial flux errors in these regions exceed the ensemble spread with values of 380 and 642 TgC year^{-1}. In Australia, the airborne observations are primarily sensitive to the southeastern part, characterized as a terrestrial carbon sink of −9 ± 67 TgC year^{-1}. The recalculated flux error in this region is also larger than the ensemble spread, estimated at 108 TgC year^{-1}. Observations in Alaska and Europe, conducted over limited periods and specific locations, mainly represent the southeastern region of Alaska and certain areas in the western Europe, with ecosystems serving as carbon sinks (−13 ± 12 and −51 ± 34 TgC year^{-1}). The estimated true flux error is larger than the ensemble spread in Europe with a value of 65 TgC year^{-1}, while it is comparatively smaller in Alaska with a value of 11 TgC year^{-1}. On the contrary, the most influential areas for the observation in Southeast Asia and South America, encompassing the western part of Southeast Asia and the northern part of Brazil, are identified as carbon sources (27 ± 118 and 603 ± 392 TgC year^{-1}, respectively). The true flux error is greater than the ensemble spread in Southeast Asia (210 TgC year^{-1}), while it is slightly lower in South America (382 TgC year^{-1}). The results indicate that the actual errors of ensemble terrestrial flux from v10 OCO-2 MIP are underestimated, particularly in regions with high anthropogenic carbon emissions.~~

4. Discussion and conclusions

~~OCO-2 MIP ensembles have given us an opportunity to understand uncertainties of inversion estimates from various error sources. As a vital evaluation tool, airborne measurements have been widely utilized in evaluating the top-down CO_2 inversion results (Houweling et al., 2015; Chevallier et al., 2019; Crowell et al., 2019; Byrne et al., 2023). Further from conventional qualitative evaluation, which compares airborne observations to posterior CO_2 concentrations, we quantitatively derive regional posterior flux errors that contribute to the observations and model differences (i.e., RMSE).~~ Our results show that the true ~~error of~~errors in the ensemble mean of posterior terrestrial ~~posterior~~ biosphere CO_2 fluxes is a major factor ~~explaining RMSE~~ contributing to the RMSE between posterior simulated CO_2 and aircraft observations for the period 2015–2017. Our findings reaffirm the feasibility of evaluating inversion performance on terrestrial biosphere flux estimates through a direct comparison between airborne observations and model data~~.~~ (Houweling et al., 2015; Chevallier et al., 2019; Crowell et al., 2019; Byrne et al., 2023). However, when evaluating inversion estimates at regional scales, the significance of representation and transport errors become pronounced. Our results show that regional variations in ~~observation~~representation errors, along with the sum of transport errors and their covariances with flux errors~~,~~ (inferred from the difference between ERR_{MIP} and $h(err_{f_e})$; Fig. S6), exceed those in true flux errors projected into CO_2 space, indicating that regional differences in *RMSE* do not directly correspond to differences in flux errors. For example, ~~on average greater observation~~although the three-year mean errors in representation and transport ~~errors of around 1.5 times~~ in East Asia ~~than~~exceed those in Southeast Asia ~~result in a significant divergence of over~~by 0.~~8~~5 and 0.3 ppm ~~in RMSE between the two~~

~~regions, despite a mere 0.2 ppm~~, respectively, the disparity in projected mean true ~~posterior~~ flux errors ~~in~~onto CO_2 space~~.~~ between the two regions is only 0.2 ppm. This result ~~could be a natural consequence as observation and~~ is supported by previous studies highlighting that the spatial distributions of simulated CO_2 concentrations can vary significantly depending on the transport ~~errors arise not only from terrestrial CO_2 fluxes but also from anthropogenic CO_2 sources and atmospheric circulation~~model (Schuch et al., ~~2019;~~ 2023) and their spatial resolution (Stanevich et al., 2020). Therefore, when utilizing airborne CO_2 measurements (and potentially other CO_2 ~~observational data~~observation) to analyze the detailed characteristics of ensemble posterior flux estimates at a regional (or latitudinal) level, it is crucial to account for the contributions of ~~observation~~representation and transport errors.

Our analysis ~~revealed~~reveals that the true errors of ensemble mean posterior fluxes is significantly greater than the ensemble spread of flux estimates in five out of seven regions. ~~This~~The underestimation ~~can be attributed to the~~ of true flux errors can arise from multiple factors, posing a challenge in determining the main cause of the ~~common~~underestimation. Possible reasons include errors in methodological assumptions and ~~observations~~atmospheric CO_2 observation commonly applied to all OCO-2 MIP ensemble members~~, which~~ because flux errors arising from these components are not captured by the ensemble spread. OCO-2 MIP models treat the fossil fuel emissions as true values and use the same dataset (i.e., ODIAC). The uncertainty of fossil fuel emissions is relatively small at national and annual scales (4-20%; Andres et al., 2014), while it becomes substantial when considering spatial distribution at model grid scale and temporal variability within a year (Zhang et al., 2016; Gurney et al., 2021). The underestimation of true flux errors only in ~~main source~~ regions~~, along~~ with ~~the absence of underestimation in Alaska and South America,~~more than three times greater fossil fuel emissions than biosphere fluxes suggests the potential presence of systematic biases originating from errors in fossil fuel emission estimates. Additionally, the regional and seasonal sampling biases of CO_2 measurements and satellite retrieval errors could contribute to these systematic biases (Kulawik et al., 2019). Eight prior flux datasets also may not adequately represent the errors of terrestrial biosphere fluxes, which exhibit significant variations among estimates (Feng et al., 2019). Therefore, further study to uncover the causes of underestimation in true flux errors is required in order to understand uncertainty sources overlooked in current ensemble inverse modeling estimates.

~~Calculated error statistics display substantial monthly variability, particularly in regions where observations are limited to specific areas.~~The reliability of our observation-based regional flux error estimates is based upon the data availability of airborne measurements. Although our approach is generally effective in estimating ~~monthly true errors of ensemble~~a regional mean ~~posterior flux,~~of monthly $h(err_{f_t})$~~,~~ it ~~faces challenges in approximately~~ is not applicable in 15% of our total cases (shown in Figure 5), when measurements were mostly made in local areas covering one to six 1°×1° grid cells within each region. This limitation may be attributed to the application of a common method for calculating observation errors across all data points, which might not adequately identify specific outliers. Caution is required when applying our approach to monthly-scale analysis, especially when using observations made ~~in local areas.~~locally. Extending the calculation period to several months or longer (e.g., Figure ~~6h~~5h) is a suitable strategy for mitigating the impact of outliers and obtaining more robust results. ~~In addition, it should be noted that the number of airborne observations used to calculate the true errors of annual ensemble terrestrial flux varied across regions. Airborne observations were concentrated in the United States and East Asia, covering a wide area with consistent monitoring. However, other regions, particularly Europe and Alaska, had sparse and intermittent data coverage. This implies that the reliability of the error estimation results in the latter case could be comparatively lower~~In fact, the ratios of three-year mean $h\left(err_{f_e}\right)$ to $h\left(err_{f_t}\right)$, which are key metrics for quantifying regional flux errors (Figure 5h), have a smaller uncertainty in mid-latitude North America and East Asia where wide and consistent airborne data are available, than over Europe and South America, where aircraft observations are sparse and only have intermittent data coverage. In addition, it is noteworthy that the $h\left(err_{f_e}\right)$ to $h\left(err_{f_t}\right)$ ratios derived from continuous observations enable the computation of unbiased true errors in the ensemble mean of annual terrestrial biosphere fluxes averaged for the analysis period, compared to those from limited observation periods (e.g., in Alaska). These results highlight the importance of having frequent airborne measurements with extensive spatial coverage for the reliable error quantification of regional terrestrial biosphere flux estimates derived from inverse models.

~~This study computes true flux errors for ensemble mean estimates by comparing RMSE and ERR_{TOT}. In this calculation, we made an assumption that the difference between $RMSE^2$ and ERR_{TOT}^2 comes from the difference between actual and estimated flux error variances. However, discrepancies between true and estimated values of not only observation~~The performance of inverse models in simulating atmospheric CO_2 may vary by season. However, airborne measurements were not uniformly conducted across all seasons in most analyzed regions. Among the seven regions analyzed, the CONTRAIL program in East Asia has continuously conducted CO_2 measurements over three years with routes repeated throughout all seasons. This has resulted in the most sensitive area to the measurements exhibiting similar spatial patterns in the NH vegetation growing season (from May to October) and non-growing season, encompassing the northeast part of China, Korea, and Japan (Fig. S7). The airborne measurements in East Asia offer a unique opportunity to explore the seasonal variations of regional error statistics. For the period of 2015–2017, the regional averages of both *RMSE* and ERR_{TOT} exhibit, on average, 12% and 11% higher values during the non-growing season compared to the growing season (Fig. S8). In contrast, the regional averages of $h\left(err_{f_e}\right)$ and $h\left(err_{f_t}\right)$ have greater values during the growing season, 0.90 [0.84, 0.97] and 1.37 [1.13, 1.62] ppm respectively, compared to the non-growing season (0.66 [0.62, 0.70] and 1.30 [1.06, 1.54] ppm) because of the tendency for CO_2 errors to increase proportionally with the magnitude of flux values. Consequently, the ratio of $h\left(err_{f_e}\right)$ to $h\left(err_{f_t}\right)$ is slightly lower during the non-growing season with 0.51 [0.39, 0.64] compared to the growing season with 0.66 [0.50, 0.83], indicating a relatively greater underestimation of true flux errors when the terrestrial biosphere CO_2 sinks are relatively smaller. This result aligns with our finding that the true terrestrial biosphere flux errors are significantly underestimated where fossil fuel emissions have larger magnitude than terrestrial biosphere fluxes.

Furthermore, the consistent ratio of $h(err_{fe})$ to $h(err_{ft})$ below 1, without significant seasonal variations in East Asia, suggests that our conclusions, drawn from the analysis of seven regions, may not be seasonally dependent.

To capture the signals from regional surface CO_2 fluxes, we used atmospheric CO_2 data observed and simulated within the 1-5 km AGL altitude range. The choice of this altitude range may influence regional error statistics, as the performance of inverse models could vary with altitude. To gauge this sensitivity, we compared error statistics derived from atmospheric CO_2 data with two altitude ranges: 1-3 km AGL and 1-5 km AGL. Among the seven analyzed regions, Australia and South America were excluded in this additional analysis because the airborne observation in these two regions cover fewer than 100 grid cells for the analysis period and narrowing the altitude range resulted in the loss of over 30% of the grid cells. The areas sensitive to airborne CO_2 measurements within the two altitude ranges exhibit nearly identical spatial patterns in Alaska, mid-latitude North America, Europe, East Asia, and Southeast Asia, indicating that observations at lower altitudes are more sensitive to surface CO_2 fluxes (Fig. S9). Because of the higher sensitivity, error statistics in all regions have larger values when calculated using data from the 1-3 km AGL altitude range compared to the 1-5 km AGL altitude range (Fig. S10). For example, in mid-latitude North America, the regional averages of *RMSE*, ERR_{TOT}, $h(err_{fe})$, and $h(err_{ft})$ are 1.42 [1.36, 1.49], 1.34 [1.30, 1.39], 0.72 [0.69, 0.76], and 0.86 [0.72, 1.01] ppm when calculated using data within the 1-3 km AGL altitude range. In comparison, when computed from the data within the 1-5 km AGL altitude range, these values are 1.21 [1.15, 1.26], 1.09 [1.06, 1.13], 0.57 [0.55, 0.60], and 0.77 [0.66, 0.88] ppm. However, the ratio of three-year mean $h(err_{fe})$ to $h(err_{ft})$ does not show significant differences based on the altitude ranges, with the difference being between 0.02 and 0.11. Again, these results suggest that our observation-based regional flux error estimates are not sensitive to the choice of altitude range for longer time periods.

Our study computes true flux errors for the ensemble mean estimates by comparing $RMSE^2$ and ERR_{TOT}^2. However, discrepancies between true and estimated values of observation, representation, and transport errors, as well as covariances between flux errors and transport errors, could contribute to variations in $RMSE^2$ and ERR_{TOT}^2. ~~First, ~~Due to a lack of information for all datasets, we set observation ~~measurement ~~errors under ideal conditions~~.~~ (i.e., 0.1 ppm). In reality, inadequate quality control can result in significant systematic ~~bias~~biases for specific regions and time periods (Masarie et al., 2011; Baier et al., 2020), impacting our results~~.~~, especially in South America. For instance, if ~~this led to an ~~the average measurement error is 0.5 ppm instead of the assumed 0.~~5~~1 ppm during the analysis period, the calculated true flux error would decrease from ~~380~~398 to 334 Tg C year^{-1} for South America and from 374 to ~~303 TgC~~260 Tg C year^{-1} for mid-latitude North America~~ and from 392 to 320 TgC year^{-1} for South America. Second, we derived observation representation error~~.

Representation errors and $h(err_{f_e})$ are derived using ~~a~~the GEOS-5 and GEOS-Chem ~~model~~models but these values depend on the transport model and meteorological ~~field~~fields used. Employing our approach across all participating MIP models to compute these two error terms and subsequently averaging them would lead to a more realistic flux error quantification in future studies. ~~In addition,~~ Employing all transport models also would facilitate the calculation of variances of flux errors and their covariance with transport errors included in ERR_{MIP} as shown in Appendix A, and subsequently enable the determination of the total true flux ~~error~~errors including both diagonal and off-diagonal terms. ~~Lastly~~In addition, previous studies show that 8-10 different ensemble members are required for robust transport error estimates (Feng et al., 2019; Lauvaux et al., 2019). However, out of the 10 ensemble members in OCO-2 MIP, three employed TM5 and five utilized GEOS-Chem (Table S1). The ensemble size might not be enough to fully capture the range of true transport errors~~,~~ ~~therefore~~. We further investigate how our main results would be affected if the estimated transport errors deviate from actual errors by 20% and 40% of the difference between $RMSE^2$ and ERR^2_{TOT}. The ratio of regional mean of $h(err_{f_e})$ to $h(err_{f_t})$ increases by, on average, only up to 0.04 and 0.09 in the seven regions throughout the analysis period, respectively (Fig. S11). In both cases, the estimated flux errors in mid-latitude North America, Europe, East Asia, and Southeast Asia still show significant underestimation at a 95% confidence level, while not in Alaska and South America. In Australia, characterized by a wide uncertainty range, significant underestimation is also observed in the 20% cases, supporting the robustness of our findings. In the future OCO-2 MIP, the participation of inverse modeling groups using other transport models or meteorological forcing data might contribute to estimating transport errors closer to actual values.

In summary, our study provides an observation-based method for quantifying errors in the ensemble ~~posterior errors~~ mean of regional terrestrial biosphere CO_2 ~~fluxes~~flux estimates which can be widely applied in inverse modeling inter-comparison projects~~, including~~ like the OCO-2 MIP. The evaluation results of the OCO-2 MIP ensemble members reveal the true errors of ensemble posterior fluxes are larger compared to the ensemble spread in regions with ~~high anthropogenic~~higher fossil fuel emissions compared to terrestrial biosphere fluxes. This finding offers important insights into understanding the sources of errors in current inverse modeling and guides future research aimed at resolving the errors in terrestrial ~~CO_2~~biosphere fluxes. Airborne observations provide a broader footprint compared to ground-based observations. Leveraging this advantage, our study ~~evaluated~~evaluates 19% of the total global land cover (excluding Antarctica and Greenland) but data scarcity ~~limited~~limits the evaluation of the remaining 81%. In addition to the ongoing airborne measurement programs including CONTRAIL, IAGOS-CARIBIC, and various airborne programs under ~~National Oceanic~~INPE, NASA, and ~~Atmospheric Administration (~~NOAA~~)~~,, airborne observations have been conducted in unexplored regions, including Siberia (e.g., Narbaud et al., 2023), Africa (e.g., Barker et al., 2020), and Northern Europe (e.g., Barker et al., 2021). The sustained efforts to maintain and expand airborne observations along with a collaborative data-sharing and management system (e.g., ObsPack) will contribute to accurately estimating and reducing the uncertainties of regional terrestrial ~~CO_2~~biosphere fluxes.

Appendix A

Following Eq. (1) in the main text,

$$RMSE^2 = \frac{1}{N}\sum_{i=1}^{N}[y_{o,i} - \overline{h(\hat{x}_i)}]\,[y_{o,i} - \overline{h(\hat{x}_i)}]^T, \qquad \text{where } \overline{h(\hat{x}_i)} = \frac{1}{M}\sum_{j=1}^{M} h_j(\hat{x}_{j,i}) \tag{A1}$$

where $\overline{h(\hat{x}_i)}$ denotes ensemble mean of posterior CO_2 concentrations in OCO-2 MIP models ~~at~~corresponding to i^{th} airborne observation ($y_{o,i}$~~).~~) within each 1°×1° grid-cell in each month. N is the total number of airborne ~~measurements~~ ~~in~~measurement data sampled at each ~~1°x1°~~ grid-cell ~~and~~monthly. M is the ensemble size (i.e., 10 members).

The Eq. (A1) can be rewritten as,

$$RMSE^2 = \frac{1}{N}\sum_{i=1}^{N}\left[\left(y_{o,i} - h_t(\hat{x}_{t,i})\right) - \left(\overline{h(\hat{x}_i)} - h_t(\hat{x}_{t,i})\right)\right]\left[\left(y_o - h_t(\hat{x}_{t,i})\right) - \left(\overline{h(\hat{x}_i)} - h_t(\hat{x}_{t,i})\right)\right]^T \tag{A2}$$

$$= \frac{1}{N}\sum_{i=1}^{N}[y_{o,i} - h_t(\hat{x}_{t,i})]\,[y_{o,i} - h_t(\hat{x}_{t,i})]^T - 2\left(y_o - h_t(\hat{x}_{t,i})\right) * \left(\overline{h(\hat{x}_i)} - h_t(\hat{x}_{t,i})\right) + [\overline{h(\hat{x}_i)} - h_t(\hat{x}_{t,i})][\overline{h(\hat{x}_i)} - h_t(\hat{x}_{t,i})]^T, \tag{A3}$$

where $h_t(\hat{x}_t)$ denotes the estimated CO_2 concentration obtained from an error-free atmospheric transport model (h_t) and true CO_2 fluxes ($\hat{x}_t$). The three terms on the right-hand side of Eq. (A3) indicate the (i) variances of observation ~~error~~and representation errors, (ii) ~~covariance~~covariances between errors of observation ~~error~~and representation and errors of flux and transport, and (iii) variances of flux and transport errors in the ensemble estimates, respectively. Assuming the independence of observation and representation errors from transport and flux errors, Eq. (A3) can be simplified to:

$$RMSE^2 = \frac{1}{N}\sum_{i=1}^{N}[y_{o,i} - h_t(\hat{x}_{t,i})]\,[y_{o,i} - h_t(\hat{x}_{t,i})]^T + [\overline{h(\hat{x}_i)} - h_t(\hat{x}_{t,i})][\overline{h(\hat{x}_i)} - h_t(\hat{x}_{t,i})]^T \tag{A4}$$

Further, the second term on the right-hand side of Eq. (A4) can be rewritten by separating the flux error and transport error terms as follows:

$$\frac{1}{N}\sum_{i=1}^{N}[\overline{h(\hat{x}_i)} - h_t(\hat{x}_{t,i})][\overline{h(\hat{x}_i)} - h_t(\hat{x}_{t,i})]^T$$

$$= \frac{1}{N}\sum_{i=1}^{N}\left[\left(\overline{h(\hat{x}_i)} - \overline{h(\hat{x}_{t,i})}\right) - \left(h_t(\hat{x}_{t,i}) - \overline{h(\hat{x}_{t,i})}\right)\right]\left[\left(\overline{h(\hat{x}_i)} - \overline{h(\hat{x}_{t,i})}\right) - \left(h_t(\hat{x}_{t,i}) - \overline{h(\hat{x}_{t,i})}\right)\right]^T \tag{A5}$$

$$= \frac{1}{N}\sum_{i=1}^{N}\left[\overline{h(\hat{x}_i)} - \overline{h(\hat{x}_{t,i})}\right]\left[\overline{h(\hat{x}_i)} - \overline{h(\hat{x}_{t,i})}\right]^T - 2\left(\overline{h(\hat{x}_i)} - \overline{h(\hat{x}_{t,i})}\right)\left(h_t(\hat{x}_{t,i}) - \overline{h(\hat{x}_{t,i})}\right) + \left[h_t(\hat{x}_{t,i}) - \overline{h(\hat{x}_{t,i})}\right]\left[h_t(\hat{x}_{t,i}) - \overline{h(\hat{x}_{t,i})}\right]^T \tag{A6}$$

The three terms on the right-hand side of Eq. (A6) indicate the (i) variances of flux ~~error~~errors in concentration space (ii) covariances between flux ~~error~~errors and transport ~~error~~errors, and (iii) variances of transport ~~error~~errors, respectively.

In ~~this study,~~OCO-2 MIP, by approximating the ensemble spread of the posterior fluxes as true errors in the mean fluxes, it assumes that the values of the first and second terms on the right-hand side of Eq. (A4) ~~are estimated by~~can be written as the sum of observation ~~representative and measurement~~ errors (ERR^2_{OBS}), representation errors (ERR^2_{REP}), and the ensemble spread of posterior CO_2 concentrations across OCO-2 MIP models (ERR_{MIP}^2), respectively~~. When the ensemble spread represents the actual ensemble mean of transport and posterior flux errors in OCO-2 MIP models, Eq (A4) can be reformulated as follows~~:

$$RMSE^2 \approx ERR_{TOT}^2 = ERR_{OBS}^2 + ERR_{REP}^2 + ERR_{MIP}^2 \quad \text{(A7)}$$

We assume that the observation errors are independent of the representation errors.

ERR_{MIP}^2 can be also rewritten by separating flux error and transport error terms as follows:

$$ERR_{MIP}^2 = \frac{1}{N}\sum_{i=1}^{N}\frac{1}{M}\sum_{j=1}^{M}\left[\overline{h(\hat{x}_i)} - h_j(\hat{x}_{j,i})\right]\left[\overline{h(\hat{x}_i)} - h_j(\hat{x}_{j,i})\right]^T \quad \text{(A8)}$$

$$= \frac{1}{N}\sum_{i=1}^{N}\frac{1}{M}\sum_{j=1}^{M}\frac{1}{M}\sum_{k=1}^{M}\left[\left(h_k(\hat{x}_{k,i}) - h_k(\hat{x}_{j,i})\right) - \left(h_j(\hat{x}_{j,i}) - h_k(\hat{x}_{j,i})\right)\right]$$
$$\left[\left(h_k(\hat{x}_{k,i}) - h_k(\hat{x}_{j,i})\right) - \left(h_j(\hat{x}_{j,i}) - h_k(\hat{x}_{j,i})\right)\right]^T \quad \text{(A9)}$$

$$= \frac{1}{N}\sum_{i=1}^{N}\frac{1}{M}\sum_{k=1}^{M}\frac{1}{M}\sum_{j=1}^{M}\left[h_k(\hat{x}_{k,i}) - h_k(\hat{x}_{j,i})\right]\left[h_k(\hat{x}_{k,i}) - h_k(\hat{x}_{j,i})\right]^T$$
$$-2\left(h_k(\hat{x}_{k,i}) - h_k(\hat{x}_{j,i})\right)\left(h_j(\hat{x}_{j,i}) - h_k(\hat{x}_{j,i})\right)$$
$$+\left[h_j(\hat{x}_{j,i}) - h_k(\hat{x}_{j,i})\right]\left[h_j(\hat{x}_{j,i}) - h_k(\hat{x}_{j,i})\right]^T \quad \text{(A10)}$$

Same as Eq. (A6), the three terms on the right-hand side of Eq. (A10) correspond to the approximated (i) variances of flux ~~error~~errors, (ii) covariances between flux ~~error~~errors and transport ~~error~~errors, and (iii) variances of transport ~~error~~errors, respectively. ~~This study assumes that the difference between $RMSE^2$ and ERR_{TOT}^2 mainly arises from the difference in the first term, the variance of flux error.~~ For the calculation of ~~this~~the first term, utilizing all participating transport models in the OCO-2 MIP would be ideal but, in this study, we ~~approximated~~approximate it using the GEOS-Chem model.

Code and Data availability

The inverse modelling results and airborne CO_2 measurement data involved in v10 OCO-2 MIP project are available at https://www.gml.noaa.gov/ccgg/OCO2_v10mip/download.php. The high-resolution global GEOS-Chem simulation results used to calculate representation error can be obtained from Brad Weir (brad.weir@nasa.gov) and Lesley Ott (lesley.e.ott@nasa.gov) upon request. The forward and adjoint sensitivity simulations for this work were conducted using the publicly available GEOS-Chem Adjoint model. The model can be downloaded from http://wiki.seas.harvard.edu/geos-chem/index.php/GEOS-Chem_Adjoint (Henze et al., 2007; last accessed: 29 Jun 2023). ODIAC fossil fuel CO_2 emission data is available at 10.17595/20170411.001.

Author contributions

JY and JL designed this study and JY performed the ~~analyses~~analysis. JL, ~~BB~~BrB, BW, KM, and ~~BB~~BiB reviewed and provided input to the manuscript. BW and LEO provided high-resolution global GEOS-Chem simulation results. KM, ~~BB~~BiB, LVG, and ~~LVG~~SCB provided airborne CO_2 observations. JY led the writing with input from all coauthors.

Competing interests

The contact author has declared that none of the authors has any competing interests.

Acknowledgements

This research was carried out at the Jet Propulsion Laboratory, California Institute of Technology, under a contract with the National Aeronautics and Space Administration (80NM0018D0004) and has been supported by the National Aeronautics and Space Administration (grant no. 20-OCOST20-0012). We are grateful for the airborne CO_2 observation data provision by NOAA, NASA-LaRC, NASA-GSFC, INPE, ~~JMA,~~ NIES, MRI, the European research infrastructure IAGOS-CARIBIC, DOE/LBNL, and Harvard University. South America airborne CO_2 measurements are supported by the European Research Council through ASICA (grant no. 649087). Observations collected at the SGP site were partly supported by the Office of Biological and Environmental Research of the US Department of Energy under contract no. DE-AC02-05CH11231 as part of the Atmospheric Radiation Measurement Program (ARM), ARM Aerial Facility, and Environmental System Science Program (ESS). We thank to C. Sweeney, K. ~~Mckain, K.~~ Davis, J. P. Digangi, M. Y. Martin, ~~B. Baier, L. V. Gatti~~, J. B. Miller, E. Gloor, W. Peters, ~~K. Saito,~~ T. Machida, H. Matsueda, Y. Sawa, T. Niwa, E. Dlugokencky, S. R. Kawa, J. B. Abshire, H. Riris, F. Obersteiner, H. Boenisch, T. Gehrlein, A. Zahn, C. Gerbig, T. Schuck, G. Chen, M. Shook, G. A. Martins, R. A. F. de Souza, B. Stephens, E. Kort, T. Ryerson, J. Peischl, K. Aikin, S. Wofsy, B. Daube, R. Commane for contributing airborne CO_2 data. We also appreciate all of the data providers of the datasets used in GEOS-Chem model simulations. Especially, we thank all research groups involved in OCO-2 MIP contributing to provide v10 OCO-2 and in ~~-~~situ CO_2 datasets and inverse modeling outputs.

References

1. Andres, R. J., Boden, T. A., and Higdon, D.: A new evaluation of the uncertainty associated with CDIAC estimates of fossil fuel carbon dioxide emission, Tellus B: ~~Chemical and Physical Meteorology,~~Chem. Phys. Meteorol., 66, 23616, https://doi.org/10.3402/tellusb.v66.23616, 2014.
2. Baier, B. C., Sweeney, C., Choi, Y., Davis, K. J., DiGangi, J. P., Feng, S., Fried, A., Halliday, H., Higgs, J., Lauvaux, T., Miller, B. R., Montzka, S. A., Newberger, T., Nowak, J. B., Patra, P., Richter, D., Walega, J., and Weibring, P.: Multispecies Assessment of Factors Influencing Regional CO_2 and CH_4 Enhancements During the Winter 2017 ACT-America Campaign, ~~Journal of Geophysical Research: Atmospheres,~~J. Geophys. Res. Atmos., 125, e2019JD031339, https://doi.org/10.1029/2019JD031339, 2020.
3. ~~Baker, I. T., Denning, A. S., and Stöckli, R.: North American gross primary productivity: regional characterization and interannual variability, 62, 533–549, , 2010.~~
3. Baier, B., Sweeney, C., Tans, P., Newberger, T., Higgs, J., and Wolter, S.: NOAA AirCore atmospheric sampling system profiles (Version 20210813), NOAA Global Monitoring Laboratory [data set], https://doi.org/10.15138/6AV0-MY81, 2021.
4. Barker, P. A., Allen, G., Gallagher, M., Pitt, J. R., Fisher, R. E., Bannan, T., Nisbet, E. G., Bauguitte, S. J.-B., Pasternak, D., Cliff, S., Schimpf, M. B., Mehra, A., Bower, K. N., Lee, J. D., Coe, H., and Percival, C. J.: Airborne measurements of fire emission factors for African biomass burning sampled during the MOYA campaign, ~~Atmospheric Chemistry and Physics,~~Atmos. Chem. Phys., 20, 15443–15459, https://doi.org/10.5194/acp-20-15443-2020, 2020.
5. Barker, P. A., Allen, G., Pitt, J. R., Bauguitte, S. J.-B., Pasternak, D., Cliff, S., France, J. L., Fisher, R. E., Lee, J. D., Bower, K. N., and Nisbet, E. G.: Airborne quantification of net methane and carbon dioxide fluxes from European Arctic wetlands in Summer 2019, ~~Philosophical Transactions of the Royal Society A: Mathematical, Physical and Engineering Sciences,~~Philos. Trans. R. Soc. A: Math. Phys. Eng. Sci., 380, 20210192, https://doi.org/10.1098/rsta.2021.0192, 2021.
6. Bastos, A., Ciais, P., Chevallier, F., Rödenbeck, C., Ballantyne, A. P., Maignan, F., Yin, Y., Fernández-Martínez, M., Friedlingstein, P., Peñuelas, J., Piao, S. L., Sitch, S., Smith, W. K., Wang, X., Zhu, Z., Haverd, V., Kato, E., Jain, A. K., Lienert, S., Lombardozzi, D., Nabel, J. E. M. S., Peylin, P., Poulter, B., and Zhu, D.: Contrasting effects of CO_2 fertilization, land-use change and warming on seasonal amplitude of Northern Hemisphere CO_2 exchange, ~~Atmospheric Chemistry and Physics,~~Atmos. Chem. Phys., 19, 12361–12375, https://doi.org/10.5194/acp-19-12361-2019, 2019.
7. Basu, S., Baker, D. F., Chevallier, F., Patra, P. K., Liu, J., and Miller, J. B.: The impact of transport model differences on CO_2 surface flux estimates from OCO-2 retrievals of column average CO_2, ~~Atmospheric Chemistry and Physics,~~Atmos. Chem. Phys., 18, 7189–7215, https://doi.org/10.5194/acp-18-7189-2018, 2018.

~~8.~~ Biraud, S. C., Torn, M. S., Smith, J. R., Sweeney, C., Riley, W. J., and Tans, P. P.: A multi-year record of airborne CO_2 observations in the US Southern Great Plains, Atmos. Meas. Tech., 6, 751–763, https://doi.org/10.5194/amt-6-751-2013~~Byrne, B., Baker, D. F., Basu, S., Bertolacci, M., Bowman, K. W., Carroll, D., Chatterjee, A., Chevallier, F., Ciais, P., Cressie, N., Crisp, D., Crowell, S., Deng, F., Deng, Z., Deutscher, N. M., Dubey, M. K., Feng, S., García, O. E., Herkommer, B., Hu, L., Jacobson, A. R., Janardanan, R., Jeong, S., Johnson, M. S., Jones, D. B. A., Kivi, R., Liu, J., Liu, Z., Maksyutov, S., Miller, J. B., Miller, S. M., Morino, I., Notholt, J., Oda, T., O'Dell, C. W., Oh, Y.-S., Ohyama, H., Patra, P. K., Peiro, H., Petri, C., Philip, S., Pollard, D. F., Poulter, B., Remaud, M., Schuh, A., Sha, M. K., Shiomi, K., Strong, K., Sweeney, C., Té, Y., Tian, H., Velazco, V. A., Vrekoussis, M., Warneke, T., Worden, J. R., Wunch, D., Yao, Y., Yun, J., Zammit-Mangion, A., and Zeng, N.: Pilot top-down CO_2 Budget constrained by the v10 OCO-2 MIP Version 1, Committee on Earth Observing Satellites [data set], https://doi.org/10.48588/npf6-sw92, Version 1.0, 2022.~~

8. , 2013.

9. Byrne, B., Baker, D. F., Basu, S., Bertolacci, M., Bowman, K. W., Carroll, D., Chatterjee, A., Chevallier, F., Ciais, P., Cressie, N., Crisp, D., Crowell, S., Deng, F., Deng, Z., Deutscher, N. M., Dubey, M. K., Feng, S., García, O. E., Griffith, D. W. T., Herkommer, B., Hu, L., Jacobson, A. R., Janardanan, R., Jeong, S., Johnson, M. S., Jones, D. B. A., Kivi, R., Liu, J., Liu, Z., Maksyutov, S., Miller, J. B., Miller, S. M., Morino, I., Notholt, J., Oda, T., O'Dell, C. W., Oh, Y.-S., Ohyama, H., Patra, P. K., Peiro, H., Petri, C., Philip, S., Pollard, D. F., Poulter, B., Remaud, M., Schuh, A., Sha, M. K., Shiomi, K., Strong, K., Sweeney, C., Té, Y., Tian, H., Velazco, V. A., Vrekoussis, M., Warneke, T., Worden, J. R., Wunch, D., Yao, Y., Yun, J., Zammit-Mangion, A., and Zeng, N.: National CO_2 budgets (2015–2020) inferred from atmospheric CO_2 observations in support of the global stocktake, Earth ~~System Science~~Syst. Sci. Data, 15, 963–1004, https://doi.org/10.5194/essd-15-963-2023, 2023.

10. Chevallier, F., Bréon, F.-M., and Rayner, P. J.: Contribution of the Orbiting Carbon Observatory to the estimation of CO_2 sources and sinks: Theoretical study in a variational data assimilation framework, ~~Journal of Geophysical Research: Atmospheres,~~J. Geophys. Res. Atmos., 112, https://doi.org/10.1029/2006JD007375, 2007.

~~11. Chevallier, F., Feng, L., Bösch, H., Palmer, P. I., and Rayner, P. J.: On the impact of transport model errors for the estimation of CO_2 surface fluxes from GOSAT observations, Geophysical Research Letters, 37, , 2010.~~

~~12.~~11. Chevallier, F., Remaud, M., O'Dell, C. W., Baker, D., Peylin, P., and Cozic, A.: Objective evaluation of surface- and satellite-driven carbon dioxide atmospheric inversions, ~~Atmospheric Chemistry and Physics,~~Atmos. Chem. Phys., 19, 14233–14251, https://doi.org/10.5194/acp-19-14233-2019, 2019.

~~13.~~12. Ciais, P., Bastos, A., Chevallier, F., Lauerwald, R., Poulter, B., Canadell, J. G., Hugelius, G., Jackson, R. B., Jain, A., Jones, M., Kondo, M., Luijkx, I. T., Patra, P. K., Peters, W., Pongratz, J., Petrescu, A. M. R., Piao, S., Qiu, C., Von Randow, C., Regnier, P., Saunois, M., Scholes, R., Shvidenko, A., Tian, H., Yang, H., Wang, X., and Zheng, B.: Definitions and methods to estimate regional land carbon fluxes for the second phase of the REgional

Carbon Cycle Assessment and Processes Project (RECCAP-2), ~~Geoscientific~~Geosci. Model ~~Development,~~Dev., 15, 1289–1316, https://doi.org/10.5194/gmd-15-1289-2022, 2022.

~~14.~~13. Crowell, S., Baker, D., Schuh, A., Basu, S., Jacobson, A. R., Chevallier, F., Liu, J., Deng, F., Feng, L., McKain, K., Chatterjee, A., Miller, J. B., Stephens, B. B., Eldering, A., Crisp, D., Schimel, D., Nassar, R., O'Dell, C. W., Oda, T., Sweeney, C., Palmer, P. I., and Jones, D. B. A.: The 2015–2016 carbon cycle as seen from OCO-2 and the global in situ network, ~~Atmospheric Chemistry and Physics,~~Atmos. Chem. Phys., 19, 9797–9831, https://doi.org/10.5194/acp-19-9797-2019, 2019.

14. Davis, K. J., Browell, E. V., Feng, S., Lauvaux, T., Obland, M. D., Pal, S., Baier, B. C., Baker, D. F., Baker, I. T., Barkley, Z. R., Bowman, K. W., Cui, Y. Y., ~~Jacobson~~Denning, A. ~~R., Feng,~~ S., ~~Wesloh, D., Barkley, Z. R., Zhang, L.~~DiGangi, J. P., Dobler, J. T., Fried, A., Gerken, T., Keller, K., ~~Baker, D~~Lin, B., Nehrir, A. R., Normile, C. P., O'Dell, C. W., Ott, L. E., Roiger, A., Schuh, A. E., Sweeney, C., Wei, Y., Weir, B., Xue, M., and ~~Davis, K. J.: Evaluation of CarbonTracker's Inverse Estimates of North American Net Ecosystem Exchange of CO_2 From Different Observing Systems Using~~ Williams, C. A.: The Atmospheric Carbon and Transport (ACT~~-~~)-America Mission, Bull. Am. Meterol. Soc., 102, E1714–E1734, https://doi.org/10.1175/BAMS-D-20-0300.1, 2021.

15. DiGangi, J. P., Choi, Y., Nowak, J. B., Halliday, H. S., Diskin, G. S., Feng, S., Barkley, Z. R., Lauvaux, T., Pal, S., Davis, K. J., Baier, B. C., and Sweeney, C.: Seasonal Variability in Local Carbon Dioxide Biomass Burning Sources Over Central and Eastern US Using Airborne ~~Observations, Journal of Geophysical Research: Atmospheres,~~In Situ Enhancement Ratios, J. Geophys. Res. Atmos., 126, ~~e2020JD034406~~e2020JD034525, https://doi.org/10.1029/~~2020JD034406~~2020JD034525, 2021.

~~16. Deng, F., Jones, D. B. A., Henze, D. K., Bousserez, N., Bowman, K. W., Fisher, J. B., Nassar, R., O'Dell, C., Wunch, D., Wennberg, P. O., Kort, E. A., Wofsy, S. C., Blumenstock, T., Deutscher, N. M., Griffith, D. W. T., Hase, F., Heikkinen, P., Sherlock, V., Strong, K., Sussmann, R., and Warneke, T.: Inferring regional sources and sinks of atmospheric~~ ~~CO_2 from GOSAT XCO_2 data, Atmospheric Chemistry and Physics, 14, 3703–3727, , 2014.~~

~~17.~~16. Feng, L., Palmer, P. I., Bösch, H., and Dance, S.: Estimating surface CO_2 fluxes from space-borne CO_2 dry air mole fraction observations using an ensemble Kalman Filter, ~~Atmospheric Chemistry and Physics,~~Atmos. Chem. Phys., 9, 2619–2633, https://doi.org/10.5194/acp-9-2619-2009, 2009.

~~18.~~17. Feng, S., Lauvaux, T., Davis, K. J., Keller, K., Zhou, Y., Williams, C., Schuh, A. E., Liu, J., and Baker, I.: Seasonal Characteristics of Model Uncertainties From Biogenic Fluxes, Transport, and Large-Scale Boundary Inflow in Atmospheric CO_2 Simulations Over North America, ~~Journal of Geophysical Research: Atmospheres,~~J. Geophys. Res. Atmos., 124, 14325–14346, https://doi.org/10.1029/2019JD031165, 2019.

~~19.~~18. Filges, A., Gerbig, C., Chen, H., Franke, H., Klaus, C., and Jordan, A.: The IAGOS-core greenhouse gas package: a measurement system for continuous airborne observations of CO_2, CH_4, H_2O and CO, Tellus B: ~~Chemical and Physical Meteorology,~~Chem. Phys. Meteorol., 67, 27989, https://doi.org/10.3402/tellusb.v67.27989, 2015.

~~20.~~19. Friedlingstein, P., O'Sullivan, M., Jones, M. W., Andrew, R. M., ~~Gregor, L~~Bakker, D. C. E., Hauck, J., Landschützer, P., Le Quéré, C., Luijkx, I. T., ~~Olsen, A.,~~ Peters, G. P., Peters, W., Pongratz, J., Schwingshackl, C., Sitch, S., Canadell, J. G., Ciais, P., Jackson, R. B., Alin, S. R., ~~Alkama, R., Arneth, A., Arora, V. K~~Anthoni, P., Barbero, L., Bates, N. R., Becker, M., Bellouin, N., ~~Bittig, H. C~~Decharme, B., Bopp, L., Brasika, I. B. M., Cadule, P., Chamberlain, M. A., Chandra, N., Chau, T.-T.-T., Chevallier, F., Chini, L. P., Cronin, M., Dou, X., Enyo, K., Evans, W., Falk, S., Feely, R. A., Feng, L., Ford, D. J., Gasser, T., ~~Gehlen, M~~Ghattas, J., Gkritzalis, T., ~~Gloege, L.,~~ Grassi, G., Gregor, L., Gruber, N., Gürses, Ö., Harris, I., Hefner, M., Heinke, J., Houghton, R. A., Hurtt, G. C., Iida, Y., Ilyina, T., Jacobson, A. R., Jain, A~~. K~~., Jarníková, T., Jersild, A., ~~Kadono, K~~Jiang, F., Jin, Z., Joos, F., Kato, E., Keeling, R. F., Kennedy, D., Klein Goldewijk, K., Knauer, J., Korsbakken, J. I., ~~Landschützer, P~~Körtzinger, A., Lan, X., Lefèvre, N., ~~Lindsay, K~~Li, H., Liu, J., Liu, Z., Ma, L., Marland, G., Mayot, N., ~~McGrath, M. J., Metzl, N., Monacci, N. M~~McGuire, P. C., McKinley, G. A., Meyer, G., Morgan, E. J., Munro, D. R., Nakaoka, S.-I., Niwa, Y., O'Brien, K~~., ~~. M., Olsen, A., Omar, A. M., Ono, T., ~~Palmer, P. I., Pan, N~~Paulsen, M., Pierrot, D., Pocock, K., Poulter, B., Powis, C. M., Rehder, G., Resplandy, L., Robertson, E., Rödenbeck, C., ~~Rodriguez, C.,~~ Rosan, T. M., Schwinger, J., Séférian, R., ~~Shutler, J. D., Skjelvan, I., Steinhoff, T., Sun, Q., Sutton, A. J., Sweeney, C., Takao, S., Tanhua, T., Tans, P. P., Tian, X., Tian, H., Tilbrook, B., Tsujino, H., Tubiello, F., van der Werf, G. R., Walker, A. P., Wanninkhof, R., Whitehead, C., Willstrand Wranne, A.,~~ et al.: Global Carbon Budget ~~2022~~2023, Earth ~~System Science~~Syst. Sci. Data, ~~14, 4811–4900~~15, 5301–5369, https://doi.org/10.5194/essd-15-5301-2023~~, 2022~~, 2023.

~~21.~~20. Gatti, L. V., Cunha, C. L., Marani, L., Cassol, H. L. G., Messias, C. G., Arai, E., Denning, A. S., Soler, L. S., Almeida, C., Setzer, A., Domingues, L. G., Basso, L. S., Miller, J. B., Gloor, M., Correia, C. S. C., Tejada, G., Neves, R. A. L., Rajao, R., Nunes, F., Filho, B. S. S., Schmitt, J., Nobre, C., Corrêa, S. M., Sanches, A. H., Aragão, L. E. O. C., Anderson, L., Von Randow, C., Crispim, S. P., Silva, F. M., and Machado, G. B. M.: Increased Amazon carbon emissions mainly from decline in law enforcement, Nature, 621, 318–323, https://doi.org/10.1038/s41586-023-06390-0, 2023.

~~22.~~21. Gelaro, R., McCarty, W., Suárez, M. J., Todling, R., Molod, A., Takacs, L., Randles, C. A., Darmenov, A., Bosilovich, M. G., Reichle, R., Wargan, K., Coy, L., Cullather, R., Draper, C., Akella, S., Buchard, V., Conaty, A., da Silva, A. M., Gu, W., Kim, G.-K., Koster, R., Lucchesi, R., Merkova, D., Nielsen, J. E., Partyka, G., Pawson, S., Putman, W., Rienecker, M., Schubert, S. D., Sienkiewicz, M., and Zhao, B.: The Modern-Era Retrospective Analysis for Research and Applications, Version 2 (MERRA-2), J. Climate, 30, 5419–5454, https://doi.org/10.1175/JCLI-D-16-0758.1, 2017.

~~23.~~22. Gurney, K. R., Law, R. M., Denning, A. S., Rayner, P. J., Pak, B. C., Baker, D., Bousquet, P., Bruhwiler, L., Chen, Y.-H., Ciais, P., Fung, I. Y., Heimann, M., John, J., Maki, T., Maksyutov, S., Peylin, P., Prather, M., and Taguchi, S.: Transcom 3 inversion intercomparison: Model mean results for the estimation of seasonal carbon sources and sinks, Global ~~Biogeochemical~~Biogeochem. Cycles, 18, https://doi.org/10.1029/2003GB002111, 2004.

~~24.~~23. Gurney, K. R., Liang, J., Roest, G., Song, Y., Mueller, K., and Lauvaux, T.: Under-reporting of greenhouse gas emissions in U.S. cities, Nat Commun, 12, 553, https://doi.org/10.1038/s41467-020-20871-0, 2021.

24. Haynes, K.D., Baker, I.T., and Denning, A.S.: SiB4 Modeled Global 0.5-Degree Monthly Carbon Fluxes and Pools, 2000-2018. ORNL DAAC, Oak Ridge, Tennessee, USA. https://doi.org/10.3334/ORNLDAAC/1848, 2021.

25. Henze, D. K., Hakami, A., and Seinfeld, J. H.: Development of the adjoint of GEOS-Chem, ~~Atmospheric Chemistry and Physics,~~Atmos. Chem. Phys., 7, 2413–2433, https://doi.org/10.5194/acp-7-2413-2007, 2007.

26. Houweling, S., Baker, D., Basu, S., Boesch, H., Butz, A., Chevallier, F., Deng, F., Dlugokencky, E. J., Feng, L., Ganshin, A., Hasekamp, O., Jones, D., Maksyutov, S., Marshall, J., Oda, T., O'Dell, C. W., Oshchepkov, S., Palmer, P. I., Peylin, P., Poussi, Z., Reum, F., Takagi, H., Yoshida, Y., and Zhuravlev, R.: An intercomparison of inverse models for estimating sources and sinks of CO_2 using GOSAT measurements, ~~Journal of Geophysical Research: Atmospheres,~~J. Geophys. Res. Atmos., 120, 5253–5266, https://doi.org/10.1002/2014JD022962, 2015.

27. Karion, A., Sweeney, C., Tans, P., and Newberger, T.: AirCore: An Innovative Atmospheric Sampling System, ~~Journal of Atmospheric and~~J. Atmos. Oceanic ~~Technology,~~Tech., 27, 1839–1853, https://doi.org/10.1175/2010JTECHA1448.1, 2010.

28. Karion, A., Sweeney, C., Wolter, S., Newberger, T., Chen, H., Andrews, A., Kofler, J., Neff, D., and Tans, P.: Long-term greenhouse gas measurements from aircraft, Atmos. Meas. Tech., 6, 511–526, https://doi.org/10.5194/amt-6-511-2013, 2013.

~~28.~~29. Kawa, S. R., Abshire, J. B., Baker, D. F., Browell, E. V., Crisp, D., Crowell, S. M. R., Hyon, J. J., Jacob, J. C., Jucks, K. W., Lin, B., Menzies, R. T., and Ott, L. E., and Zaccheo, T. S.: Active Sensing of CO_2 Emissions over Nights, Days, and Seasons (ASCENDS): Final Report of the ASCENDS Ad Hoc Science Definition Team, Document ID: 20190000855, NASA/TP–2018-219034, GSFC-E-DAA-TN64573, 2018.

~~29.~~30. Kulawik, S. S., Crowell, S., Baker, D., Liu, J., McKain, K., Sweeney, C., Biraud, S. C., Wofsy, S., O'Dell, C. W., Wennberg, P. O., Wunch, D., Roehl, C. M., Deutscher, N. M., Kiel, M., Griffith, D. W. T., Velazco, V. A., Notholt, J., Warneke, T., Petri, C., De Mazière, M., Sha, M. K., Sussmann, R., Rettinger, M., Pollard, D. F., Morino, I., Uchino, O., Hase, F., Feist, D. G., Roche, S., Strong, K., Kivi, R., Iraci, L., Shiomi, K., Dubey, M. K., Sepulveda, E., Rodriguez, O. E. G., Té, Y., Jeseck, P., Heikkinen, P., Dlugokencky, E. J., Gunson, M. R., Eldering, A., Crisp, D., Fisher, B., and Osterman, G. B.: Characterization of OCO-2 and ACOS-GOSAT biases and errors for CO_2 flux estimates, Atmospheric Measurement Techniques Discussions, 1–61, https://doi.org/10.5194/amt-2019-257, 2019.

~~30.~~31. Lauvaux, T., Díaz-Isaac, L. I., Bocquet, M., and Bousserez, N.: Diagnosing spatial error structures in CO_2 mole fractions and XCO_2 column mole fractions from atmospheric transport, ~~Atmospheric Chemistry and Physics,~~Atmos. Chem. Phys., 19, 12007–12024, https://doi.org/10.5194/acp-19-12007-2019, 2019.

~~31.~~32. Liu, J., Bowman, K. W., Lee, M., Henze, D. K., Bousserez, N., Brix, H., James Collatz, G., Menemenlis, D., Ott, L., Pawson, S., Jones, D., and Nassar, R.: Carbon monitoring system flux estimation and attribution: impact of ACOS-GOSAT XCO_2 sampling on the inference of terrestrial biospheric sources and sinks, Tellus B: ~~Chemical and Physical Meteorology,~~Chem. Phys. Meteorol., 66, 22486, https://doi.org/10.3402/tellusb.v66.22486, 2014.

~~32.~~33. Liu, J., Bowman, K. W., and Henze, D. K.: Source-receptor relationships of column-average CO_2 and implications for the impact of observations on flux inversions, ~~Journal of Geophysical Research: Atmospheres,~~J. Geophys. Res. Atmos., 120, 5214–5236, https://doi.org/10.1002/2014JD022914, 2015.

~~33.~~34. Liu, J., Bowman, K. W., Schimel, D. S., Parazoo, N. C., Jiang, Z., Lee, M., Bloom, A. A., Wunch, D., Frankenberg, C., Sun, Y., O'Dell, C. W., Gurney, K. R., Menemenlis, D., Gierach, M., Crisp, D., and Eldering, A.: Contrasting carbon cycle responses of the tropical continents to the 2015–2016 El Niño, Science, 358, eaam5690, https://doi.org/10.1126/science.aam5690, 2017.

~~34.~~35. Liu, J., Baskaran, L., Bowman, K., Schimel, D., Bloom, A. A., Parazoo, N. C., Oda, T., Carroll, D., Menemenlis, D., Joiner, J., Commane, R., Daube, B., Gatti, L. V., McKain, K., Miller, J., Stephens, B. B., Sweeney, C., and Wofsy, S.: Carbon Monitoring System Flux Net Biosphere Exchange 2020 (CMS-Flux NBE 2020), Earth ~~System Science~~Syst. Sci. Data, 13, 299–330, https://doi.org/10.5194/essd-13-299-2021, 2021.

~~35.~~36. Machida, T., Matsueda, H., Sawa, Y., Nakagawa, Y., Hirotani, K., Kondo, N., Goto, K., Nakazawa, T., Ishikawa, K., and Ogawa, T.: Worldwide Measurements of Atmospheric CO_2 and Other Trace Gas Species Using Commercial Airlines, ~~Journal of Atmospheric and~~J. Atmos. Oceanic ~~Technology,~~Tech., 25, 1744–1754, https://doi.org/10.1175/2008JTECHA1082.1, 2008.

~~36.~~37. Masarie, K. A., Pétron, G., Andrews, A., Bruhwiler, L., Conway, T. J., Jacobson, A. R., Miler, J.B., Tans, P. P., Worthy, D. E., and Peters, W.: Impact of CO_2 measurement bias on CarbonTracker surface flux estimates. ~~Journal of Geophysical Research: Atmospheres,~~J. Geophys. Res. Atmos., 116, D17, https://doi.org/10.1029/2011JD016270, 2011.

38. Miller, J. B., Martins, G. A., de Souza, R. A., and Schuldt, K. N.: Manaus Aircraft profile data for the period 2017-2020; obspack_multi-species_1_manaus_profiles_v1.0_202105-19, NOAA Global Monitoring Laboratory [data set], https://doi.org/10.25925/20210519, 2021.

~~37.~~39. Nara, H., Tanimoto, H., Tohjima, Y., Mukai, H., Nojiri, Y., and Machida, T.: Emission factors of CO_2, CO and CH_4 from Sumatran peatland fires in 2013 based on shipboard measurements, Tellus B~~,~~: Chem. Phys. Meteorol., 69, 1399047, https://doi.org/10.1080/16000889.2017.1399047, 2017.

~~38.~~40. Narbaud, C., Paris, J.-D., Wittig, S., Berchet, A., Saunois, M., Nédélec, P., Belan, B. D., Arshinov, M. Y., Belan, S. B., Davydov, D., Fofonov, A., and Kozlov, A.: Disentangling methane and carbon dioxide sources and transport across the Russian Arctic from aircraft measurements, ~~Atmospheric Chemistry and Physics,~~Atmos. Chem. Phys., 23, 2293–2314, https://doi.org/10.5194/acp-23-2293-2023, 2023.

41. NOAA Carbon Cycle Group ObsPack Team: INPE atmospheric carbon dioxide data for the period 2015-2017, obspack_co2_1_INPE_RESTRICTED_v2.0_2018-11-13, NOAA Earth System Research Laboratory, Global Monitoring Division, http://dx.doi.org/10.25925/20181030, 2018.

42. Oda and Maksyutov, ODIAC Fossil Fuel CO_2 Emissions Dataset (Version name: ODIAC2020b), Center for Global Environmental Research, National Institute for Environmental Studies, doi:10.17595/20170411.001, 2015. (Reference date: 2022/05/14)

~~39.~~43. O'Dell, C. W., Eldering, A., Wennberg, P. O., Crisp, D., Gunson, M. R., Fisher, B., Frankenberg, C., Kiel, M., Lindqvist, H., Mandrake, L., Merrelli, A., Natraj, V., Nelson, R. R., Osterman, G. B., Payne, V. H., Taylor, T. E., Wunch, D., Drouin, B. J., Oyafuso, F., Chang, A., McDuffie, J., Smyth, M., Baker, D. F., Basu, S., Chevallier, F., Crowell, S. M. R., Feng, L., Palmer, P. I., Dubey, M., García, O. E., Griffith, D. W. T., Hase, F., Iraci, L. T., Kivi, R., Morino, I., Notholt, J., Ohyama, H., Petri, C., Roehl, C. M., Sha, M. K., Strong, K., Sussmann, R., Te, Y., Uchino, O., and Velazco, V. A.: Improved retrievals of carbon dioxide from Orbiting Carbon Observatory-2 with the version 8 ACOS algorithm, Atmos. Meas. Tech., 11, 6539–6576, https://doi.org/10.5194/amt-11-6539-2018, 2018.

~~40.~~44. Peiro, H., Crowell, S., Schuh, A., Baker, D. F., O'Dell, C., Jacobson, A. R., Chevallier, F., Liu, J., Eldering, A., Crisp, D., Deng, F., Weir, B., Basu, S., Johnson, M. S., Philip, S., and Baker, I.: Four years of global carbon cycle observed from the Orbiting Carbon Observatory 2 (OCO-2) version 9 and in situ data and comparison to OCO-2 version 7, ~~Atmospheric Chemistry and Physics,~~Atmos. Chem. Phys., 22, 1097–1130, https://doi.org/10.5194/acp-22-1097-2022, 2022.

~~41.~~45. Philip, S., Johnson, M. S., Potter, C., Genovesse, V., Baker, D. F., Haynes, K. D., Henze, D. K., Liu, J., and Poulter, B.: Prior biosphere model impact on global terrestrial CO_2 fluxes estimated from OCO-2 retrievals, ~~Atmospheric Chemistry and Physics,~~Atmos. Chem. Phys., 19, 13267–13287, https://doi.org/10.5194/acp-19-13267-2019, 2019.

~~42.~~46. Piao, S., Wang, X., Wang, K., Li, X., Bastos, A., Canadell, J. G., Ciais, P., Friedlingstein, P., and Sitch, S.: Interannual variation of terrestrial carbon cycle: Issues and perspectives, ~~Global~~Glob. Change ~~Biology,~~Biol., 26, 300–318, https://doi.org/10.1111/gcb.14884, 2020.

~~43. Randerson, J. T., Van Der Werf, G. R., Giglio, L., Collatz, G. J., & Kasibhatla, P. S. (2015). Global Fire Emissions Database, Version 4, (GFEDv4), ORNL DAAC, Oak Ridge, Tennessee, USA.~~

47. Rodgers, C. D.: Inverse Methods for Atmospheric Sounding: Theory and Practice, World Scientific, River Edge, USA, ISBN 978-9810227401, 2000.

~~44.~~48. Schuh, A. E., Jacobson, A. R., Basu, S., Weir, B., Baker, D., Bowman, K., Chevallier, F., Crowell, S., Davis, K. J., Deng, F., Denning, S., Feng, L., Jones, D., Liu, J., and Palmer, P. I.: Quantifying the Impact of Atmospheric Transport Uncertainty on CO_2 Surface Flux Estimates, Global ~~Biogeochemical~~Biogeochem. Cycles, 33, 484–500, https://doi.org/10.1029/2018GB006086, 2019.

49. Schuldt, K. N., Jacobson, A. R., Aalto, T., Andrews, A., Bakwin, P., Bergamaschi, P., Biermann, T., Biraud, S. C., Chen, H., Colomb, A., Conil, S., Cristofanelli, P., De Mazière, M., De Wekker, S., Delmotte, M., Dlugokencky, E., Emmenegger, L., Fischer, M. L., Hatakka, J., Heliasz, M., Hermanssen, O., Holst, J., Jaffe, D., Karion, A., Kazan, V., Keronen, P., Kominkova, K., Kubistin, D., Laurent, O., Laurila, T., Lee, J., Lehner, I., Leuenberger, M., Lindauer,

M., Lopez, M., Mammarella, I., Manca, G., Marek, M. V., McKain, K., Miller, J. B., Miller, C. E., Myhre, C. L., Mölder, M., Müller-Williams, J., Piacentino, S., Pichon, J. M., Plass-Duelmer, C., Ramonet, M., Scheeren, B., Schumacher, M., Sha, M. K., Sloop, C. D., Smith, P., Steinbacher, M., Sweeney, C., Tans, P., Thoning, K., Trisolino, P., Tørseth, K., Viner, B., Vitkova, G., and di Sarra, A. G.: Multi-laboratory compilation of atmospheric carbon dioxide data for the years 2020–2021; obspack_co2_1_NRT_v6.1.1_2021-05-17, NOAA Earth System Research Laboratory, Global Monitoring Laboratory [data set], https://doi.org/10.25925/20210517, 2021a.

~~45.~~50. Schuldt, K. N., Mund, J., Luijkx, I. T., Aalto, T., Abshire, J. B., Aikin, K., Andrews, A., Aoki, S., Apadula, F., Baier, B., Bakwin, P., Bartyzel, J., Bentz, G., Bergamaschi, P., Beyersdorf, A., Biermann, T., Biraud, S. C., Boenisch, H., Bowling, D., Brailsford, G., Chen, G., Chen, H., Chmura, L., Clark, S., Climadat, S., Colomb, A., Commane, R., Conil, S., Cox, A., Cristofanelli, P., Cuevas, E., Curcoll, R., Daube, B., Davis, K., Mazière, M. D., De Wekker, S., Della Coletta, J., Delmotte, M., DiGangi, J. P., Dlugokencky, E., Elkins, J. W., Emmenegger, L., Fang, S., Fischer, M. L., Forster, G., Frumau, A., Galkowski, M., Gatti, L. V., Gehrlein, T., Gerbig, C., Gheusi, F., Gloor, E., Gomez-Trueba, V., Goto, D., Griffis, T., Hammer, S., Hanson, C., Haszpra, L., Hatakka, J., Heimann, M., Heliasz, M., Hensen, A., Hermanssen, O., Hintsa, E., Holst, J., Jaffe, D., Joubert, W., Karion, A., Kawa, S. R., Kazan, V., Keeling, R., Keronen, P., Kolari, P., Kominkova, K., Kort, E., Kozlova, E., Krummel, P., Kubistin, D., Labuschagne, C., Lam, D. H., Langenfelds, R., Laurent, O., Laurila, T., Lauvaux, T., Law, B., Lee, O. S., Lee, J., Lehner, I., Leppert, R., Leuenberger, M., Levin, I., Levula, J., Lin, J., Lindauer, M., Loh, Z., Lopez, M., Machida, T., Mammarella, I., Manca, G., Manning, A., Manning, A., Marek, M. V., Martin, M. Y., Matsueda, H., McKain, K., Meijer, H., Meinhardt, F., Merchant, L., Mihalopoulos, N., Miles, N., Miller, C. E., Miller, J. B., Mitchell, L., Montzka, S., Moore, F., Morgan, E., Morgui, J.-A., Morimoto, S., Munger, B., Myhre, C. L., Mölder, M., Obersteiner, F., M uller-Williams, J., Necki, J., Newman, S., Nichol, S., Niwa, Y., O'Doherty, S., Paplawsky, B., Peischl, J., Peltola, O., Pichon, J. M., Piper, S., Plass-Duelmer, C., Ramonet, M., Ramos, R., Reyes-Sanchez, E., Richardson, S., Riris, H., Rivas, P. P., Ryerson, T., Saito, K., Sargent, M., Sasakawa, M., Sawa, Y., Say, D., Scheeren, B., Schuck, T., Schumacher, M., Seifert, T., Sha, M. K., Shepson, P., Shook, M., Sloop, C. D., Smith, P., Steinbacher, M., Stephens, B., Sweeney, C., Tans, P., Thoning, K., Timas, H., Torn, M., Trisolino, P., Turnbull, J., Tørseth, K., Vermeulen, A., Viner, B., Vitkova, G., Walker, S., Watson, A., Wofsy, S., Worsey, J., Worthy, D., Young, D., Zahn, A., Zimnoch, M., van Dinther, D., and van den Bulk, P.: Multi-laboratory compilation of atmospheric carbon dioxide data for the period 1957–2019; obspack_co2_1_GLOBALVIEWplus_v6.1_2021-03-01, NOAA Earth System Research Laboratory, Global Monitoring Laboratory [data set], https://doi.org/10.25925/20201204, ~~2021~~2021b.

~~46.~~51. Stanevich, I., Jones, D. B. A., Strong, K., Parker, R. J., Boesch, H., Wunch, D., Notholt, J., Petri, C., Warneke, T., Sussmann, R., Schneider, M., Hase, F., Kivi, R., Deutscher, N. M., Velazco, V. A., Walker, K. A., and Deng, F.: Characterizing model errors in chemical transport modeling of methane: impact of model resolution in versions v9-02 of GEOS-Chem and v35j of its adjoint model, ~~Geoscientific~~Geosci. Model ~~Development,~~Dev., 13, 3839–3862, https://doi.org/10.5194/gmd-13-3839-2020, 2020.

~~47.~~52. Stephens, B. B., Long, M. C., Keeling, R. F., Kort, E. A., Sweeney, C., Apel, E. C., Atlas, E. L., Beaton, S., Bent, J. D., Blake, N. J., Bresch, J. F., Casey, J., Daube, B. C., Diao, M., Diaz, E., Dierssen, H., Donets, V., Gao, B.-C., Gierach, M., Green, R., Haag, J., Hayman, M., Hills, A. J., Hoecker-Martínez, M. S., Honomichl, S. B., Hornbrook, R. S., Jensen, J. B., Li, R.-R., McCubbin, I., McKain, K., Morgan, E. J., Nolte, S., Powers, J. G., Rainwater, B., Randolph, K., Reeves, M., Schauffler, S. M., Smith, K., Smith, M., Stith, J., Stossmeister, G., Toohey, D. W., and Watt, A. S.: The O_2/N_2 Ratio and CO_2 Airborne Southern Ocean Study, ~~Bulletin of the American Meteorological Society,~~Bull. Am. Meteorol. Soc., 99, 381–402, https://doi.org/10.1175/BAMS-D-16-0206.1, 2018.

~~48.~~53. Sweeney, C., Karion, A., Wolter, S., Newberger, T., Guenther, D., Higgs, J. A., Andrews, A. E., Lang, P. M., Neff, D., Dlugokencky, E., Miller, J. B., Montzka, S. A., Miller, B. R., Masarie, K. A., Biraud, S. C., Novelli, P. C., Crotwell, M., Crotwell, A. M., Thoning, K., and Tans, P. P.: Seasonal climatology of CO_2 across North America from aircraft measurements in the NOAA/ESRL Global Greenhouse Gas Reference Network, ~~Journal of Geophysical Research: Atmospheres,~~J. Geophys. Res. Atmos., 120, 5155–5190, https://doi.org/10.1002/2014JD022591, 2015.

54. Sweeney, C., Chatterjee, A., Wolter, S., McKain, K., Bogue, R., Conley, S., Newberger, T., Hu, L., Ott, L., Poulter, B., Schiferl, L., Weir, B., Zhang, Z., and Miller, C. E.: Using atmospheric trace gas vertical profiles to evaluate model fluxes: a case study of Arctic-CAP observations and GEOS simulations for the ABoVE domain, Atmos. Chem. Phys., 22, 6347–6364, https://doi.org/10.5194/acp-22-6347-2022, 2022.

55. Thompson, C. R., Wofsy, S. C., Prather, M. J., Newman, P. A., Hanisco, T. F., Ryerson, T. B., Fahey, D. W., Apel, E. C., Brock, C. A., Brune, W. H., Froyd, K., Katich, J. M., Nicely, J. M., Peischl, J., Ray, E., Veres, P. R., Wang, S., Allen, H. M., Asher, E., Bian, H., Blake, D., Bourgeois, I., Budney, J., Bui, T. P., Butler, A., Campuzano-Jost, P., Chang, C., Chin, M., Commane, R., Correa, G., Crounse, J. D., Daube, B., Dibb, J. E., DiGangi, J. P., Diskin, G. S., Dollner, M., Elkins, J. W., Fiore, A. M., Flynn, C. M., Guo, H., Hall, S. R., Hannun, R. A., Hills, A., Hintsa, E. J., Hodzic, A., Hornbrook, R. S., Huey, L. G., Jimenez, J. L., Keeling, R. F., Kim, M. J., Kupc, A., Lacey, F., Lait, L. R., Lamarque, J.-F., Liu, J., McKain, K., Meinardi, S., Miller, D. O., Montzka, S. A., Moore, F. L., Morgan, E. J., Murphy, D. M., Murray, L. T., Nault, B. A., Neuman, J. A., Nguyen, L., Gonzalez, Y., Rollins, A., Rosenlof, K., Sargent, M., Schill, G., Schwarz, J. P., Clair, J. M. S., Steenrod, S. D., Stephens, B. B., Strahan, S. E., Strode, S. A., Sweeney, C., Thames, A. B., Ullmann, K., Wagner, N., Weber, R., Weinzierl, B., Wennberg, P. O., Williamson, C. J., Wolfe, G. M., and Zeng, L.: The NASA Atmospheric Tomography (ATom) Mission: Imaging the Chemistry of the Global Atmosphere, Bull. Am. Meteorol. Soc., 103, E761–E790, https://doi.org/10.1175/BAMS-D-20-0315.1, 2022.

~~49.~~56. Tohjima, Y., Mukai, H., Machida, T., Nojiri, Y., and Gloor, M.: First measurements of the latitudinal atmospheric O_2 and CO_2 distributions across the western Pacific, Geophys. Res. Lett., 32, L17805, https://doi.org/10.1029/2005GL023311, 2005.

~~50.~~57. Tomohiro Oda, Shamil Maksyutov (2015), ODIAC Fossil Fuel CO_2 Emissions Dataset (Version name: ODIAC2020b), Center for Global Environmental Research, National Institute for Environmental Studies, doi:10.17595/20170411.001. (Reference date: 2023/04/01)

58. Vay, S. A., Tyler, S. C., Choi, Y., Blake, D. R., Blake, N. J., Sachse, G. W., Diskin, G. S., and Singh, H. B.: Sources and transport of $\Delta^{14}C$ in CO_2 within the Mexico City Basin and vicinity, Atmos. Chem. Phys., 9, 4973–4985, https://doi.org/10.5194/acp-9-4973-2009, 2009.

~~51.~~ Wei, Y., R. Shrestha, S. Pal, T. Gerken, S. Feng, J. McNelis, D. Singh, M. M. Thornton, A. G. Boyer, M. A. Shook, G. Chen, B. C. Baier, Z. R. Barkley, J. D. Barrick, J. R. Bennett, E. V. Browell, J. F. Campbell, L. J. Campbell, Y. Choi, J. Collins, J. Dobler, M. Eckl, A. Fiehn, A. Fried, J. P. Digangi, R. Barton-Grimley, H. Halliday, T. Klausner, S. Kooi, J. Kostinek, T. Lauvaux, B. Lin, M. J. McGill, B. Meadows, N. L. Miles, A. R. Nehrir, J. B. Nowak, M. Obland, C. O'Dell, R. M. P. Fao, S. J. Richardson, D. Richter, A. Roiger, C. Sweeney, J. Walega, P. Weibring, C. A. Williams, M. M. Yang, Y. Zhou, and K. J. Davis, 2021, Atmospheric Carbon and Transport – America (ACT-America) Datasets: Description, Management, and Delivery, Earth Space Sci, 8, e2020EA001634, https://doi.org/10.1029/2020EA001634~~Tsuboi, K., Matsueda, H., Sawa, Y., Niwa, Y., Nakamura, M., Kuboike, D., Saito, K., Ohmori, H., Iwatsubo, S., Nishi, H., Hanamiya, Y., Tsuji, K., and Baba, Y.: Evaluation of a new JMA aircraft flask sampling system and laboratory trace gas analysis system, Atmospheric Measurement Techniques, 6, 1257–1270, , 2013.~~

59. , 2021.

~~52.~~60. Weir, B., Crisp, D., O'Dell, C. W., Basu, S., Chatterjee, A., Kolassa, J., Oda, T., Pawson, S., Poulter, B., Zhang, Z., Ciais, P., Davis, S. J., Liu, Z., and Ott, L. E.: Regional impacts of COVID-19 on carbon dioxide detected worldwide from space, ~~Science Advances,~~Sci. Adv., 7, eabf9415, https://doi.org/10.1126/sciadv.abf9415, 2021.

61. Yun, J., Jeong, S., Gruber, N., Gregor, L., Ho, C.-H., Piao, S., Ciais, P., Schimel, D., and Kwon, E. Y.: Enhance seasonal amplitude of atmospheric CO_2 by the changing Southern Ocean carbon sink, Sci. Adv., 8, eabq0220, https://doi.org/10.1126/sciadv.abq0220, 2022.

~~53.~~62. Zhang, X., Gurney, K. R., Rayner, P., Baker, D., and Liu, Y.-P.: Sensitivity of simulated CO_2 concentration to sub-annual variations in fossil fuel CO_2 emissions, Atmos. Chem. Phys., 16, 1907–1918, https://doi.org/10.5194/acp-16-1907-2016, 2016.